JOURNAL OF PETROLOGY | VOLUME 45 | NUMBER 10 | PAGES 1983–2009 | 2004 | doi:10.1093/petrology/egh045

Quantifying Three-Dimensional Silicate Fabrics in Cumulates Using Cumulative Distribution Functions

JEFFREY S. GEE[1]*, WILLIAM P. MEURER[2], PETER A. SELKIN[1] AND MICHAEL J. CHEADLE[3]

[1]GEOSCIENCES RESEARCH DIVISION, SCRIPPS INSTITUTION OF OCEANOGRAPHY, LA JOLLA, CA 92093-0220, USA

[2]DEPARTMENT OF GEOSCIENCES, UNIVERSITY OF HOUSTON, HOUSTON, TX 77204-5007, USA

[3]DEPARTMENT OF GEOLOGY AND GEOPHYSICS, UNIVERSITY OF WYOMING, LARAMIE, WY 82701, USA

RECEIVED MAY 1, 2003; ACCEPTED MAY 5, 2004
ADVANCE ACCESS PUBLICATION AUGUST 12, 2004

We present a new method for quantifying three-dimensional silicate fabrics and the associated uncertainties from grain orientation data on three orthogonal sections. Our technique is applied to the orientation of crystallographic features and, hence, yields a fabric related to the lattice-preferred orientation, although the method could be applied to shape-preferred orientations or strain analysis based on passive linear markers. The orientation data for each section are represented by their cumulative distribution function, and an iterative procedure is used to find the symmetric second-rank strain tensor that will simultaneously satisfy the cumulative distribution functions observed on each section. For samples with well-developed fabrics, this technique provides a much closer match to the sectional data than do previous techniques based on eigenparameter analysis of two-dimensional orientation data. Robust uncertainty estimates are derived from a non-parametric bootstrap resampling scheme. The method is applied to two cumulates: one with a well-developed fabric and the other with a weak fabric, from the Stillwater complex, Montana. The silicate petrofabric orientations obtained for these samples compare favorably with independent direct estimates of the volume fabric from electron backscatter diffraction and magnetic techniques.

KEY WORDS: *cumulates; fabrics; quantitative; Stillwater complex; textural analysis*

INTRODUCTION

Fractional crystallization (the segregation of crystals from liquid or vice versa) is a central concept in our understanding of magmatic evolution and magma chamber processes. Although much can be inferred about magmatic evolution from the compositions of rocks and minerals, the textures of cumulates provide the only direct record of the physical processes involved. Recently, there has been a substantial increase in the number and type of quantitative textural studies of cumulates. These include studies of crystal-size distributions (e.g. Waters & Boudreau, 1996; Higgins, 1998, 2002; Zieg & Marsh, 2002), spatial distribution patterns of grains (e.g. Jerram *et al.*, 1996; Jerram & Cheadle, 2000), and fabric analyses (Higgins, 1991; Meurer & Boudreau, 1998*a*, 1998*b*). However, a major limitation to understanding the textures of cumulates is the lack of a standard method for collecting orientation data and quantifying three-dimensional (3D) fabrics.

A number of workers have discussed methods for calculating the 3D fabric (or strain) ellipsoid from sectional ellipse data on three or more planes (see review by Robin, 2002). The two-dimensional (2D) sectional ellipse data may be estimated from the shapes of deformed ellipsoidal particles (Ramsay, 1967; Shimamoto & Ikeda, 1976) or from eigenvalue analysis of linear passive markers (Woodcock, 1977; Harvey & Laxton, 1980). The final 3D ellipsoid is then calculated under the assumption that the sectional ellipses represent sections through the same average ellipsoid. We refer to this technique of constructing the 3D ellipsoid from 2D ellipses as the sectional ellipse method.

Despite its importance and widespread use in fabric and structural studies, the sectional ellipse method has

*Corresponding author. Telephone: (858) 534-4707. Fax: (858) 534-0784. E-mail: jsgee@ucsd.edu

several limitations. In many types of analysis (e.g. where grain or crystallographic orientations constitute the basic 2D data), only the axial ratio and orientation of each sectional ellipse is determined. These ellipses must then be adjusted for compatibility at their mutual intersections prior to calculation of the 3D ellipsoid (e.g. De Paor, 1990). Even when sectional ellipse areas, or, equivalently, the absolute lengths of the ellipse axes, are available, Wheeler (1986) has argued that the sectional ellipses need not represent compatible sections through the average ellipsoid. Finally, and perhaps most importantly for practical applications, this method depends critically on preparing sections within the principal planes of the ellipsoid. Identification of these planes is often not possible and, as illustrated below, even minor deviations from these principal planes can cause significant errors in samples with pronounced fabrics.

In this contribution, we present a new method for quantifying 3D silicate fabrics and the associated uncertainties from orientation data on three orthogonal sections. The orientation data for each section are represented by their cumulative distribution function (CDF), the monotonic function representing the cumulative probability of a particular orientation with respect to the reference axis of the thin section (Rice, 1995). An iterative procedure is used to find the symmetric second-rank strain tensor that, when applied to a large number of unit vectors uniformly distributed on a sphere, will simultaneously satisfy the CDFs observed on each orthogonal section. The 3D-orientation matrix representing this deformed distribution provides the desired description of the fabric. A non-parametric bootstrap resampling scheme (Efron, 1982; Constable & Tauxe, 1990) is used to provide error estimates on the eigenvectors and eigenvalues of the orientation matrix.

Our aim is to present a method for the quantitative description of the 3D arrangement of crystals in rocks, and not a method to determine strain. However, because the fabric is quantified relative to an assumed initial homogeneous fabric, the calculated strain tensor will be related to the sum of the (homogeneous irrotational) strain that the sample experienced if the sample had an initially random distribution of crystals. If the initial distribution was not random or is not known (as is commonly the case), then the calculated strain tensor cannot be taken as a measure of strain. Interpretation of strain is further complicated by the behavior of rigid crystals during deformation. Nonetheless, the orientation matrix of the deformed distribution produced by this strain tensor still provides a quantitative description of how the sample's fabric departs from a uniform distribution.

The CDF technique provides a 3D fabric estimate from 2D linear features and, hence, is suitable for description of shape-preferred or lattice-preferred orientations (SPO and LPO, respectively) and is ideal for strain analysis based on passive linear markers. Here, we focus primarily on the application of the CDF technique to the orientation of crystallographic features (traces of twin planes or cleavages) to derive a crystallographic fabric. This fabric compares favorably with direct estimates of the crystallographic fabric from electron backscatter diffraction (EBSD). We examine the effect of weighting the individual orientation data by grain length or area as a way to provide a more representative estimate of the volume fabric. We also illustrate how the CDF technique may be used to determine SPO fabrics and compare the results of our approach with fabrics derived from image analysis and the intercept-counting technique (Launeau *et al.*, 1990). Finally, we compare the 3D silicate fabrics with magnetic fabric estimates that may serve as proxies for the orientation and degree of silicate fabric development.

THE STRAIN TENSOR AND THE ORIENTATION MATRIX

The goal of quantitative fabric studies is to provide a description of grain orientations, ideally summarized by a small number of parameters suitable for statistical comparisons. Two related representations of the fabric are possible: (1) the orientation matrix that provides a simple statistical description of the orientation and degree of clustering of the grains, and (2) the strain tensor that will transform an initially uniform distribution into the preferred orientation distribution observed. In the 2D case, the eigenvalues of the orientation matrix give a direct estimate of the strain ratio of the deformed distribution and the eigenvector associated with the major eigenvalue gives the orientation of the principal strain axis (Harvey & Laxton, 1980). For a 3D distribution of linear markers, however, the situation is more complex. Although the eigenvectors of the orientation matrix track those of the strain tensor (Woodcock, 1977), the eigenvalues of the orientation matrix deviate from the corresponding strain tensor eigenvalues (Harvey & Laxton, 1980). In this section, we briefly review the differences between these two possible representations of the 3D fabric and illustrate limitations of the sectional ellipse method.

If complete orientation information (i.e. all three direction cosines) is available for a set of linear markers, the orientation matrix provides a convenient description of the 3D fabric (Scheidegger, 1965; Watson, 1966; Woodcock, 1977). Consider a collection of n linear markers (e.g. representing the crystallographic c-axis of a grain), each of which is treated as a unit vector, with direction cosines (x_i, y_i, z_i). The direction cosines may be used to form the

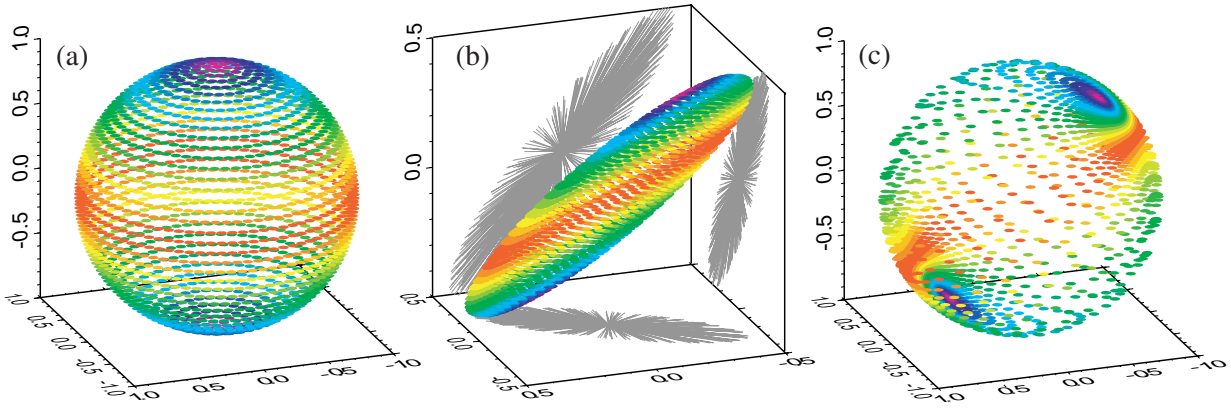

Fig. 1. Deformation of a uniform 3D distribution of unit vectors by application of a strain tensor. (a) Initial uniform distribution of unit vectors. Vector endpoint color is proportional to the z coordinate. (b) Deformed 3D distribution after application of prolate strain tensor and projections of these vectors (decimated by 5 for clarity) onto three orthogonal planes. (c) Distribution from (b) as unit vectors. The direction cosines of these unit vectors are used to construct the orientation matrix.

symmetric matrix

$$G_{3D} = \frac{1}{n}\begin{bmatrix} \sum x_i^2 & \sum x_i y_i & \sum x_i z_i \\ \sum x_i y_i & \sum y_i^2 & \sum y_i z_i \\ \sum x_i z_i & \sum y_i z_i & \sum z_i^2 \end{bmatrix}$$

which has been termed the 'normalized cosine dispersion matrix' or the 'orientation matrix'. The three eigenvectors ($\mathbf{v}_1$, $\mathbf{v}_2$, $\mathbf{v}_3$) and the corresponding eigenvalues ($g_1 \geq g_2 \geq g_3$) of G_{3D} give information on the orientation and degree of clustering of the data. In particular, the eigenvector corresponding to the maximum eigenvalue gives the orientation about which the moment of inertia of the distribution is minimum, i.e. the direction about which the largest number of grain orientations is clustered (Watson, 1966). Note that the three eigenvalues of G_{3D} will always be positive and, when normalized by the number of grains as above, will sum to 1 (Watson, 1966). The shape and magnitude of the preferred orientation can, therefore, be visualized as a real ellipsoid (Nye, 1957), which we refer to as the orientation or fabric ellipsoid, with principal semi-axis lengths of $g_1 \geq g_2 \geq g_3$.

Alternatively, the 3D distribution of linear passive markers may be described in terms of the strain tensor that would transform an initially uniform distribution into the observed orientation distribution. A symmetric second-rank strain tensor (S_{ij}) is applied to each vector in the uniform distribution ($\mathbf{u}_i$) to yield a vector in the deformed distribution ($\mathbf{d}_i$):

$$\begin{bmatrix} S_{11} & S_{12} & S_{13} \\ S_{12} & S_{22} & S_{23} \\ S_{13} & S_{23} & S_{33} \end{bmatrix} \cdot \begin{bmatrix} u_x \\ u_y \\ u_z \end{bmatrix} = \begin{bmatrix} d_x \\ d_y \\ d_z \end{bmatrix}.$$

In general, these deformed vectors will differ both in orientation and length relative to the unit vectors of the initial uniform distribution (Fig. 1). For simplicity, we will consider only changes in the distributions of directions of the deformed vectors (Fig. 1c).

This forward modeling technique provides a simple method of investigating the relationship between the orientation matrix and the strain tensor [see Harvey & Laxton (1980) for a more comprehensive discussion of this relationship]. Comparison of the eigenvalue ratios for the orientation matrix and the strain tensor (Fig. 2a) reveals that the eigenvalue ratios of the orientation matrix are always greater than or equal to the corresponding eigenvalue ratios for the strain tensor. The magnitude of this discrepancy is a function of the fabric shape. Thus, the degree of preferred orientation as estimated from the eigenvalues of G_{3D} might be significantly different for samples with oblate and prolate fabrics, even though both fabrics resulted from the same amount of strain. The orientation matrix provides a more anisotropic representation of the fabric than does the strain tensor, but as the strain tensor may be calculated from the orientation matrix (and vice versa), either may be used to describe the preferred orientation.

Although some techniques (e.g. universal stage or EBSD) provide full 3D orientation data, more commonly orientation data are available only on planar sections and these sectional data are combined using the sectional ellipse technique. The forward modeling technique outlined above can also be used to evaluate the suitability of the sectional ellipse technique. The projection of each individual grain orientation from the deformed 3D distribution onto three orthogonal planes is calculated in the standard fashion [$\mathbf{v}_{proj} = \mathbf{v} - (\mathbf{v} \cdot \hat{\mathbf{n}})\hat{\mathbf{n}}$, where $\hat{\mathbf{n}}$ is the normal to the plane]. This is equivalent to measuring the orientations of grains from a given distribution on three

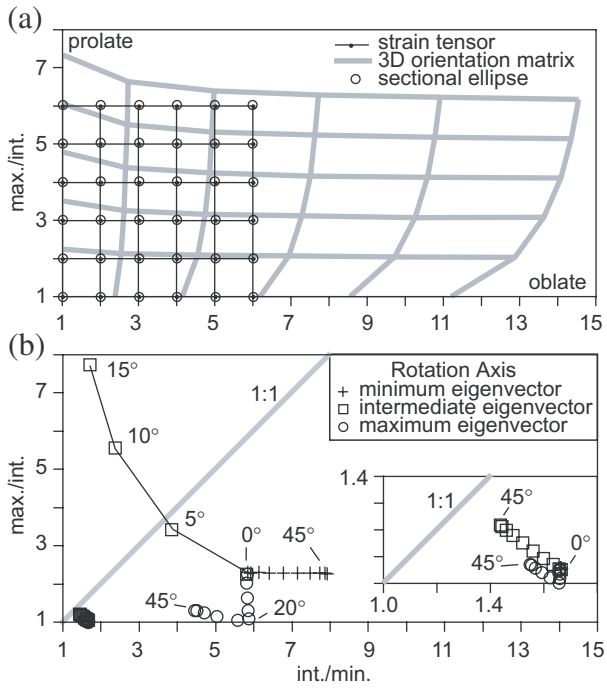

Fig. 2. Flinn-type (eigenvalue ratio) diagrams, illustrating the relationship between strain tensor, orientation tensor and 3D tensor, reconstructed by the sectional ellipse method. (a) Variation in eigenvalue ratios for the strain tensor (fine grid) and the orientation matrix (thick grey grid) that describes the orientation of unit vectors after application of the strain tensor. For planar sections cut parallel to the principal planes of the strain tensor, the sectional ellipse method (open circles) essentially recovers the 3D strain tensor. (b) Eigenvalue ratio plot of 3D tensor reconstructed using the sectional ellipse method when sections are not parallel to the principal planes. Trajectories (at 5° intervals) are shown for rotations about each of the three eigenvectors of the strain tensor. The two examples shown are for strain tensors with eigenvalue ratios approximating those determined for samples PP074 (max/int = 2·28; int/min = 5·84) and PP046 (max/int = 1·06; int/min = 1·66; inset).

orthogonal thin sections: the angular distributions of these projected vectors in each plane are used to construct the sectional ellipses. We have implemented the method described by Launeau & Cruden (1998), with the addition of a compatibility stretch (e.g. De Paor, 1990) for the sectional ellipses (here, determined from eigenvalue analysis of unit vectors), and applied it to a variety of deformed distributions (circles in Fig. 2a). When the principal planes of the strain ellipsoid are parallel to the reference planes (Fig. 2a), the sectional ellipse method essentially recovers the strain tensor.

The sectional ellipse method fares less well when applied to sections not parallel to the principal planes of the strain or fabric ellipsoid (Fig. 2b). To illustrate this point, we examine the 3D strain tensor recovered from analysis of grain orientations on orthogonal sections at variable orientations to the principal planes of the strain tensor. The particular strain tensor chosen (with semi-axis lengths of 0·66, 0·29 and 0·05; eigenvalue ratios of maximum:intermediate (L) = 2·28, intermediate:minimum (F) = 5·84) corresponds to that determined for one of the test specimens discussed below. The magnitude of anisotropy is typical of many cumulates from the Stillwater complex. The orientation of the tensor relative to the planar sections was varied by rotation about one of the principal axes of the strain tensor. For a rotation about the minimum axis of the strain tensor (i.e. two planar sections include the minimum principal axis), the resulting 3D tensor accurately recovers the ratio of the maximum to intermediate eigenvalue but not the ratio of the intermediate to minimum eigenvalue. For rotation about the maximum eigenvector, the reconstructed 3D tensor is nearly perfectly oblate for a 20° rotation and becomes more tri-axial with further rotation. The most profound effects are evident with a rotation about the intermediate axis of the tensor, corresponding to sections cut at an oblique angle to the foliation plane. Even modest deviations (5°) are sufficient to result in substantial inaccuracies in the recovered 3D tensor. We emphasize that these errors in the reconstructed 3D tensor are not a function of the closure errors resulting from the compatibility adjustment. The RMS misfit of the sectional ellipses at their common intersections is <0·5% (measured as a percentage of the sum of the intersection lengths) in all cases, and often <0·1%. Though less pronounced, similar deviations are evident for less anisotropic fabrics (Fig. 2b, inset; L = 1·06, F = 1·66 corresponding to the weaker fabric in the second test sample discussed below).

From the above analysis, we conclude that the sectional ellipse method is poorly suited for reconstructing 3D strain or fabric tensors of samples with well-developed fabrics. The necessity of preparing thin sections within the principal planes has been briefly mentioned by some workers (e.g. Launeau & Cruden, 1998), but the importance of this constraint has not been emphasized. Although the foliation plane may be readily identified in many cumulate rocks, detection of any lineation to guide the selection of thin section planes is often not possible. Even where such features can be detected prior to preparing thin sections, it is not evident that the sections could be prepared accurately enough (better than 5°) to avoid the effects illustrated above.

QUANTIFYING 3D FABRICS USING CUMULATIVE DISTRIBUTION FUNCTIONS

The relationship between the strain tensor and the orientation matrix discussed above suggests a simple method of quantifying 3D fabrics from observations on 2D sections. The angular orientation distribution on any 2D section may be predicted by applying a strain tensor to

a large number of uniformly distributed unit vectors on a sphere and subsequently projecting each grain orientation in the deformed distribution onto the observation planes (Fig. 1b). In this section, we will use this forward modeling approach to iteratively solve for the best-fit 3D strain tensor that will simultaneously satisfy the observed sectional orientation distributions. Having found this strain tensor, we will adopt the 3D orientation matrix of the corresponding deformed distribution as our preferred descriptor of the 3D fabric. The motivation for using the orientation matrix, rather than the strain tensor that is usually sought in structural studies, is twofold. First, the orientation matrix will be most directly comparable with full 3D orientation data acquired by EBSD. Secondly, the eigenvalues of G_{3D} are always positive, allowing the description of the fabric in terms of a real ellipsoid, even when the strain tensor has one or more negative eigenvalues.

We begin by reviewing the collection and analyses of the 2D orientation data (traces of crystallographic features) and the representation of these data by their CDFs. Next, we outline the procedure for estimating the best-fit strain tensor, and, hence, the orientation matrix, that will satisfy the observed CDFs. The difficulties inherent in combining sectional ellipses (Wheeler, 1986) are avoided by simultaneously fitting the cumulative distribution functions of grain orientations on each orthogonal section. We then describe the non-parametric bootstrap technique used to evaluate errors for the eigenvectors and eigenvalues of the orientation matrix. A flow chart of the various stages of data analysis is available at the *Journal of Petrology* website, http://www.petrology.oupjournals.org. Finally, we examine the justification for, and the effects of, various weighting schemes (by grain length and area) in estimating the volume fabric. Two gabbronorites from the Stillwater complex, Montana—one well foliated and the other weakly foliated—are used to demonstrate the various stages of the data analysis.

Crystallographic orientation data

The two samples used to illustrate our method of fabric analysis were collected as large oriented blocks from Olivine-bearing zone III of the Middle Banded Series (PP046, Fig. 3a) and from Olivine-bearing zone V of the Upper Banded Series (PP074, Fig. 3b) of the Stillwater complex, Montana. Both samples were collected on Picket Pin Mt, in portions of the stratigraphy with well-developed modal layering (McCallum *et al.*, 1980; Meurer & Boudreau, 1996). Both samples are extremely fresh, with less than 1% alteration. For each block, a series of single-pass cuts yielded a single square corner and three slabs suitable for preparation of oversized (75mm × 50 mm) thin sections. Although the saw cuts are nearly orthogonal (~2°), trimming and thin section production introduce additional orientation errors. We estimate the combined orientation uncertainty as ~5°.

The orientation data used in the following analysis are traces of crystallographic features in the orthogonal sections, rather than simply the grain elongation. As discussed below, these data allow an approximation of the LPO fabric to be reconstructed. The samples considered here are composed of orthopyroxene, clinopyroxene and plagioclase. Both pyroxenes have two sets of cleavages that contain the *c*-axis (Fig. 4), but, in each case, one of these cleavage directions is prominent. For clinopyroxene, the prominent cleavage also corresponds to the direction of fine exsolution lamellae and both of these features invariably correspond to the long dimension of sub- and euhedral grains. This direction is taken as the projection of the *c*-axis onto the section plane. The cleavage is less developed in the orthopyroxene and exsolution, when present, is blebby; however, in the samples analyzed, most orthopyroxene grains are nearly euhedral, allowing us to use the grain shape in combination with the cleavage to define the *c*-axis projection. Thus, our grain-tracing data for pyroxenes should reflect the *c*-axis fabric, with the minimum eigenvector of the fabric ellipsoid corresponding to the pole to the foliation and the maximum eigenvector representing the mean orientation of the pyroxene *c*-axis distribution.

We use the trace of the albite twin planes as our crystallographic reference for plagioclase (Fig. 4). The albite twin planes developed in the plagioclase ($An_{72–80}$) are orthogonal to the *b*-axis and define the trace of the *a*–*c* crystallographic plane in the thin section. Because the trace of the albite twin plane constitutes the basic data, only the minimum eigenvector of the fabric ellipsoid necessarily has any crystallographic significance (reflecting the mean orientation of the poles to {010} planes—approximately, the crystallographic *b*-axis). The tabular nature of plagioclase grains means that our tracings of the *a*–*c* plane implicitly include some additional information from the grain shapes. Specifically, our tracing of the *a*–*c* plane should approximate the orientation of the grain elongation within the *a*–*c* plane. To simplify the discussion, we will assume this elongation coincides with the *c*-axis direction (i.e. tabular grains $c > a > b$ with $c \gg b$), although we are aware that plagioclase elongation parallel to the *a*-axis is also possible. In combination with the tabular shape of the plagioclase grains, the maximum eigenvector of the fabric ellipsoid will often constitute a good approximation of the crystallographic axis parallel to the longest dimension of the grains (*c*-axis).

The three orthogonal sections were captured digitally in both plane- and cross-polarized light, using a flatbed scanner and polarizing sheets. The captured images are approximately 4050 pixels × 2700 pixels, in 32-bit color

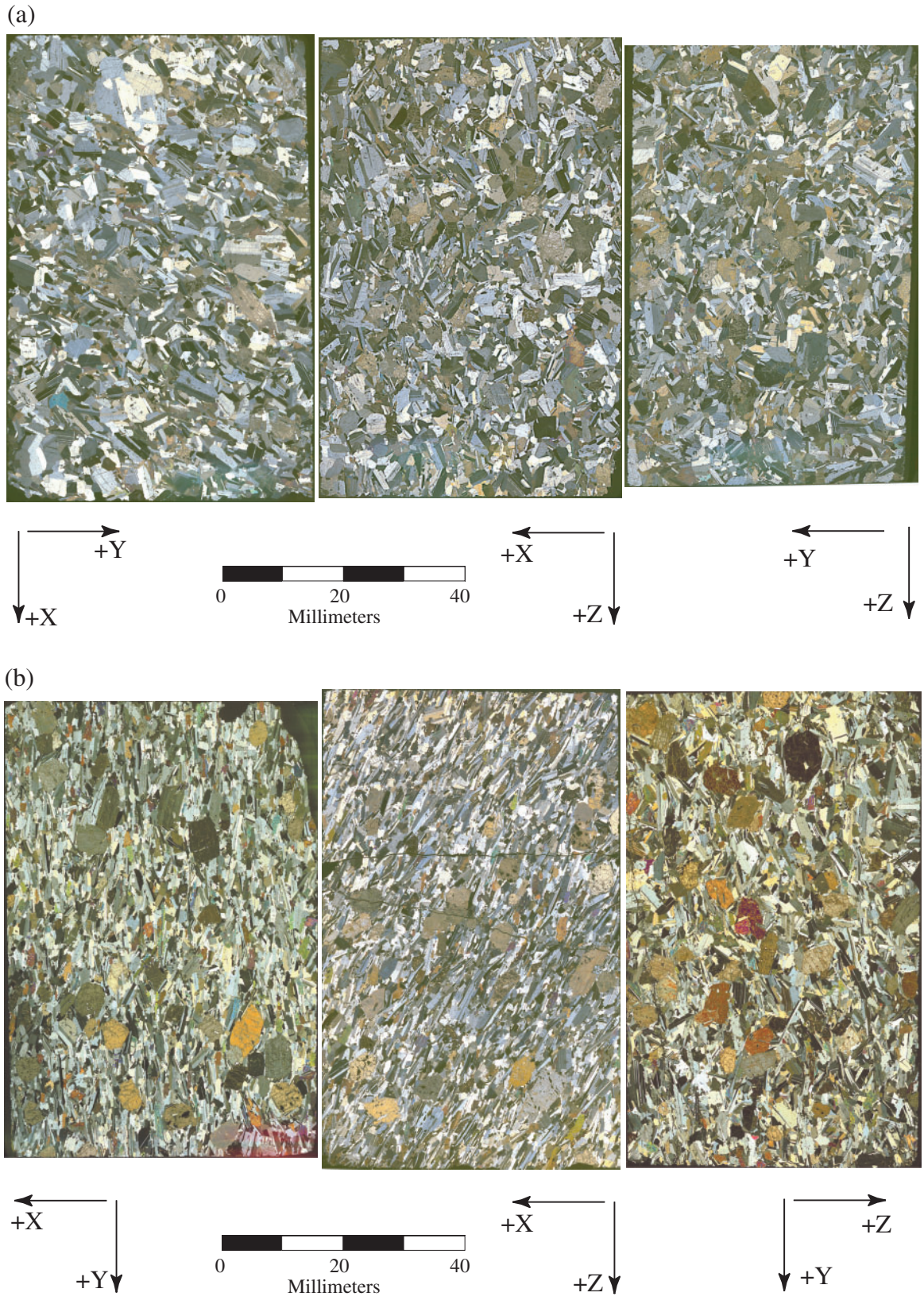

Fig. 3. Photomicrographs of orthogonal sections for samples (a) PP046 and (b) PP074.

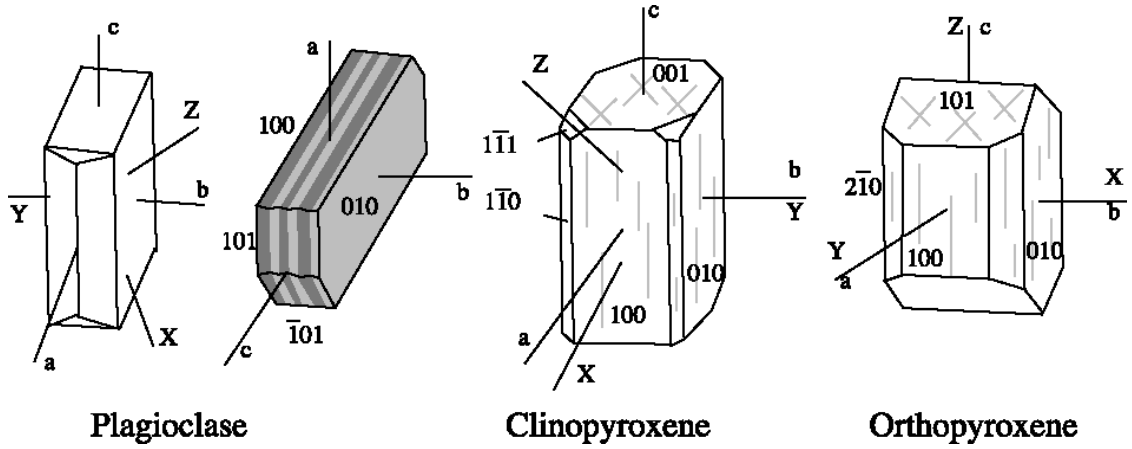

Fig. 4. Crystallography of phases used for grain tracing. For clinopyroxene and orthopyroxene, the intersection cleavage is parallel to the *c*-axis and this intersection cleavage trace serves as the basic orientation data. For plagioclase, the trace of the *a*–*c* plane (albite twin plane) in the section constitutes the basic data.

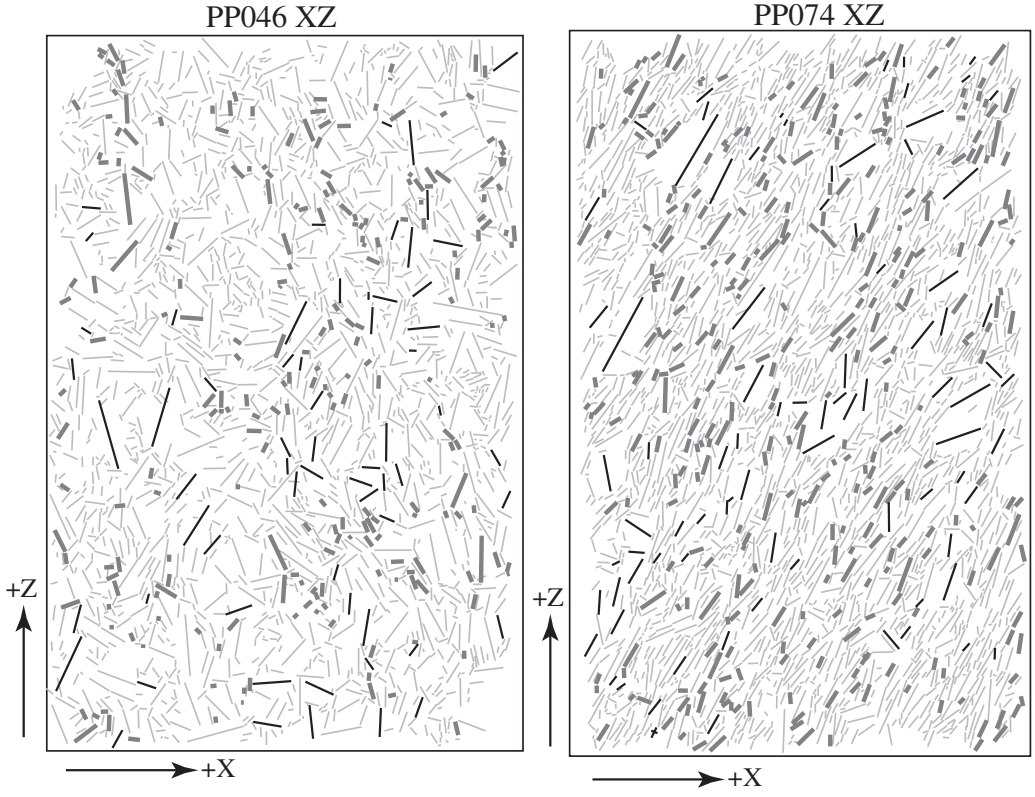

Fig. 5. Crystallographic traces for a sample with modest fabric (PP046 $X\mathcal{Z}$ plane) and a sample with a pronounced fabric (PP074 $X\mathcal{Z}$ plane). Thin grey lines represent the trace of the plagioclase *a*–*c* plane; medium black and thick dark grey lines represent the trace of the intersection cleavage in orthopyroxene and clinopyroxene, respectively. The long axis of the section is ~75 mm and the short axis is ~50 mm.

and are 46 megabyte files. For each section, the orientation and grain length were manually traced in a graphical analysis program, generating an image of the section defined by the crystallographic directions and lengths of the grains in these directions (Fig. 5). These images are then processed using NIH Image (freeware available through the US National Institute of Health) that determines the length, X–$\mathcal{Y}$ position and orientation of each grain trace and tabulates the data. For each section, angles (0°–180°) are recorded relative to the reference axis of the thin section (e.g. $X\mathcal{Y}$ plane, $+X = 0°$, $+\mathcal{Y} = 90°$).

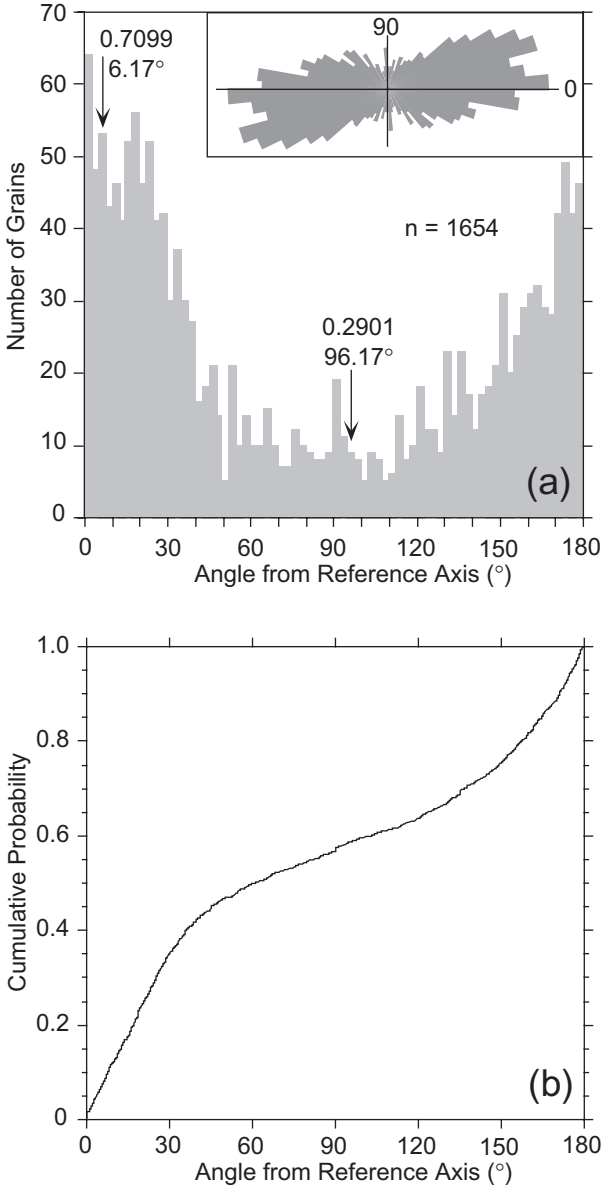

Fig. 6. Representations of 2D orientation data. (a) Histogram of angular orientations. Locations and magnitudes of maximum and minimum eigenvalues shown for reference. Inset shows rose diagram of the same data. (b) Cumulative distribution function for the same data. The curve represents the sum of all grains (normalized by the total number of grains) with orientations less than or equal to the angular value.

Calculation of 3D fabric

The 2D angular orientation data described above may be represented in several ways. These data may be graphically represented by a histogram or rose diagram (Fig. 6a). In the sectional ellipse technique, the eigenvalues and eigenvectors of the 2D orientation distribution would be used to define the sectional ellipse axial ratio and orientation. The histogram data could, in principle, be used as the input for the iterative forward calculation to find the best-fit strain tensor that simultaneously satisfies observations on three orthogonal sections. However, use of the histogram representation has one significant drawback, namely that the original data must be binned. The arbitrary selection of bin size can significantly affect the resulting 3D strain tensor, particularly for sections where a relatively small number of observations are available.

The CDF provides a more suitable representation of the 2D orientation data (Fig. 6b). For a collection of angular orientations (a_1, a_2 ... a_n) treated as unit vectors, the CDF is simply the probability that a grain orientation is less than or equal to some angle and is given by

$$CDF(\alpha) = \frac{\text{no. grains with angle} \leq \alpha}{\text{total number of grains}} = \sum_{a_i \leq \alpha} \frac{1}{n}. \quad (1)$$

Thus, the CDF is a function that monotonically increases from 0 to 1. The value is constant between successive samples (sorted into increasing order) and steps up by $1/n$ at each sample position. The CDF representation has several advantages. In contrast to histograms, the CDF requires no binning of the data. For large numbers of observations (e.g. the 1500–3000 plagioclase orientations typically available from each oversized thin section), the CDF approximates a smooth curve. For sections with few observations, the CDF will be represented by a series of coarser steps. In addition, the CDF represents an unbinned distribution of a single variable and, hence, is suitable for statistical tests comparing two distributions (e.g. Kolmogorov–Smirnov test, Press *et al.*, 1989). One might, for example, test whether the fabric in a block sample is homogeneous by comparing CDFs from subsamples of the same thin section (see below) or from two parallel thin sections.

The CDFs from the three orthogonal sections constitute the observations used to solve for the 3D strain tensor (and the accompanying orientation matrix). Using the Nelder–Mead simplex multivariate minimization technique (Press *et al.*, 1989), we iteratively solve for the six independent elements of the strain tensor that will minimize the misfit with all three CDFs (Fig. 7a). The simplex method is well suited for this application, as it requires no a priori knowledge of the derivatives of the function to be minimized. At each iteration, a test strain tensor is applied to an initial uniform distribution to produce a distribution of deformed model vectors (Fig. 1). The projections of each model vector are taken onto the three orthogonal thin section planes and the angles measured in the same fashion as for the original data.

The resulting angular distributions of model vectors in the XY, XZ and YZ planes form the basis for comparison with the original sectional orientation data. The CDFs for each distribution of model vectors are calculated as for

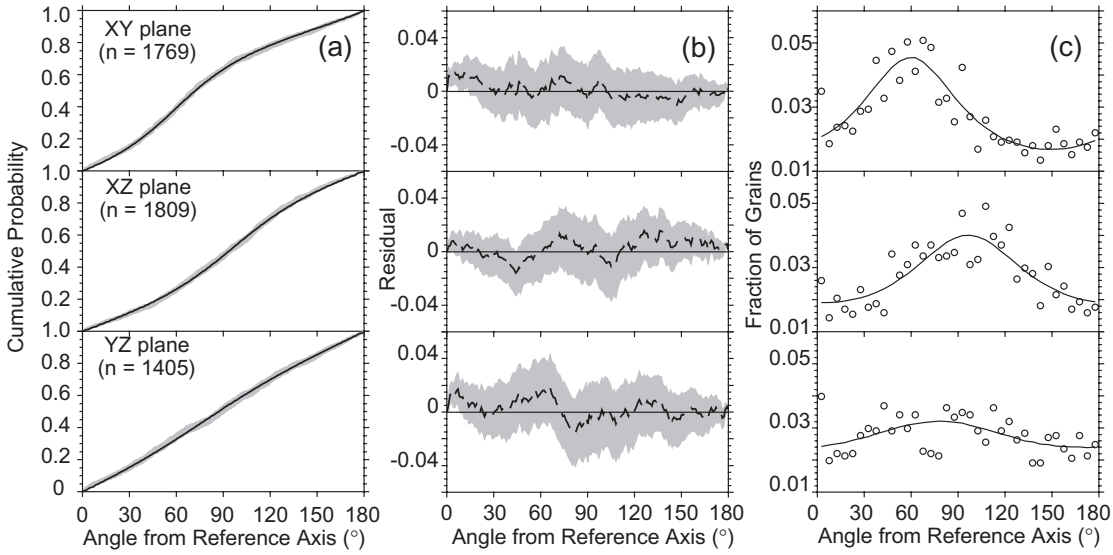

Fig. 7. Sectional data for unweighted plagioclase fabric (*a–c* planes) for sample PP046. (a) Cumulative distribution functions (CDFs) for each orthogonal section. The grey band indicates the 95% bounds on CDFs of 500 pseudosamples drawn from the original data. Black line indicates the CDF produced by the best-fit strain tensor. (b) Residuals (data – model) for each section. Thin dashed line and grey band indicate the mean and 95% bounds of the residual, respectively. (c) Comparison of original orientation data (circles) and orientation distribution predicted from best-fit tensor (line). Original data were binned at 5° intervals.

the original data (i.e. the projected model vectors are also treated as unit vectors). The CDFs for both the data and model are sampled at 1° intervals and the RMS misfit for each section is calculated. The overall misfit for all three sections is given by

$$RMS_{total} = \sqrt{RMS_{XY}^2 + RMS_{XZ}^2 + RMS_{YZ}^2}. \qquad (2)$$

It is this combined RMS misfit that is minimized in the simplex routine (see the Appendix for further details on this minimization procedure). The best-fit strain tensor is then used to calculate the 3D orientation matrix of the corresponding deformed distribution. The eigenparameters of the orientation matrix indicate the intensity and orientation of the fabric (Fig. 8 and Table 1).

Having found the best-fit tensor, it is instructive to graphically compare the predicted and observed angular orientation distributions on each section (Fig. 7c). Histograms of the original orientation data provide the most familiar format for examining how well the model fits the data. The angular histogram is simply the derivative of the CDF. For comparison with the best-fit model, we bin the original orientation data in 5° intervals that are large enough to contain a significant number of observations and yield a relatively smooth histogram. For sample PP046, the relatively weak fabric yields significant scatter in the binned orientation data. Nonetheless, the predicted distribution of orientations provides a qualitatively satisfying fit to these scattered data.

Non-parametric error estimates

The best-fit 3D orientation matrix calculated above is most useful when accompanied by error estimates on both the eigenvalues and eigenvectors of this matrix. We have no a priori knowledge of the underlying distribution for the orientation data. However, the large number of observations available on each section (typically >1500 for dominant phase and several hundred for other phases) is well suited for a non-parametric estimate of uncertainties (e.g. Constable & Tauxe, 1990). Given n orientation measurements from a section, a pseudosample of equal size is generated by a uniform random resampling procedure (i.e. a random integer is drawn from the set $\{1,2,\ldots n\}$ and the corresponding orientation observation is added to the pseudosample until the final size is reached). Thus, any individual orientation measurement may occur once, more than once or not at all in the pseudosample. Similar pseudosamples are generated for each of the three thin sections, the CDFs for each section are calculated, and the simplex minimization procedure is used to find the best-fit strain tensor and corresponding 3D orientation matrix for this pseudosample. The process is repeated a sufficiently large number of times (typically 500) to map out the uncertainties in the eigenparameters of G_{3D}. The 95% confidence bounds may then be directly determined from an ordered list of the eigenvalues or from estimating the parameters of the Kent distribution (ellipses) that enclose 95% of the eigenvectors (Fig. 8).

The uncertainty estimates provide a means to evaluate the statistical significance of the fabric shape. For

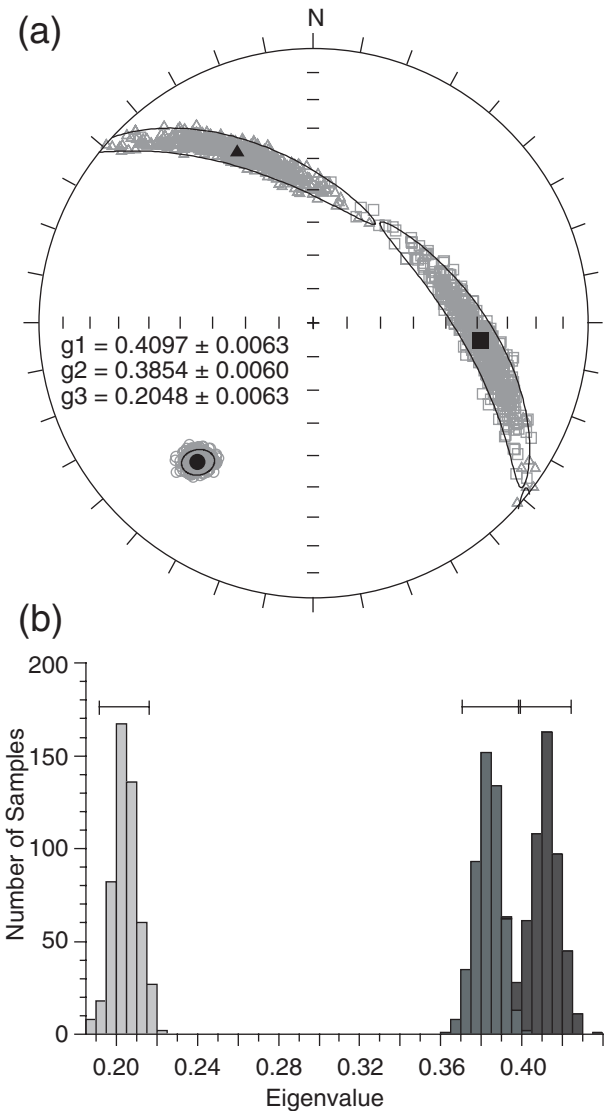

Fig. 8. Plagioclase fabric (*a*–*c* planes, unit weights) for sample PP046. (a) Lower hemisphere equal area plot of mean eigenvectors (black symbols: square, maximum; triangle, intermediate; circle, minimum), pseudosamples (grey) and 95% confidence bounds determined from bootstrap resampling. Mean eigenvalues and 1σ errors shown for reference. Note that the mean eigenparameters determined from the pseudosamples differ slightly from the best-fit values (Table 1). (b) Histogram of eigenvalues for the 500 pseudosamples. Horizontal bars indicate 95% confidence bounds from sorted eigenvalues.

example, comparison of the intermediate and maximum eigenvalues and their associated uncertainties indicates that sample PP046 has a statistically significant lineation at the 95% confidence level. In this case, the significance of the lineation is readily apparent, as the 95% confidence bounds on the maximum and intermediate eigenvalues do not overlap (Fig. 8b). When the confidence limits are larger, the statistical distinction between any two eigenvalues could be rigorously assessed using a *t*-test on the two distributions (e.g. Constable & Tauxe, 1990). The confidence bounds on the eigenvectors (Fig. 8a) provide a complementary representation of the statistical significance of the lineation in this sample.

The bootstrap resampling procedure provides additional information on the variability inherent in the sectional data, as well as a measure of the misfit between the original data and best-fit model (Fig. 7). The 500 pseudosamples generated for each section illustrate the variability that might be expected in the CDFs for different realizations of the underlying distribution from which the original sectional data are drawn. That is, the range of CDFs shows the variability that might be encountered by simply preparing thin sections from slightly different locations within the block sample. As with the eigenvalues for the 3D orientation matrix, an ordered list of the cumulative probability at any angle from the 500 pseudosamples can be used to empirically determine the 95% confidence bounds on the sectional CDFs (Fig. 7a). The residuals (observed CDF – predicted CDF from best-fit tensor) for each section allow assessment of any significant deviations between the model and data (Fig. 7b). The 95% confidence envelope on these residuals is calculated from the bounds on the sectional CDF data minus the predicted CDF from the best-fit tensor. For sample PP046, deviations significant at the 95% confidence level occur over a small angular range on the XY and YZ sections. Although the residuals for this sample are small, the pattern of residuals should reveal subfabrics within the sectional data that could, in principle, be used as the basis for fitting more complex models (e.g. bimodal distributions).

Weighting schemes

Although the treatment of grain orientation data as unit vectors yields a valuable estimate of the fabric, additional estimates that take the variability in grain length or area into account may be more suitable for comparison with independent estimates of the volume fabric. For example, crystallographic orientations obtained by EBSD are often acquired from a grid of points on a thin section and, thus, approximate an area-weighted representation of the fabric. It is also possible that grain size will be important in determining the response of a collection of grains to deformation processes. The CDF method is easily adapted to incorporate variable weights for each orientation observation. In constructing the CDF from an ordered list of the orientation measurements, the cumulative probability value is simply incremented by the weighting value of the grain (normalized by the sum of all the grain weights) rather than by $1/n$. Again, the model vectors of the deformed distribution are treated identically to the original data (i.e. if the original data are length-weighted, then the model vectors are also length-weighted in constructing the model CDFs). The minimization

Table 1: Summary of fabric results

Phase	Type	g_1	1σ	Dec	Inc	g_2	1σ	Dec	Inc	g_3	1σ	Dec	Inc
PP046 grain tracings													
Plag	UW	0·4095	0·0063	93·9	40·4	0·3855	0·0060	334·0	30·4	0·2050	0·0063	220·0	34·7
	LW	0·3908	0·0047	78·7	45·2	0·3743	0·0050	326·0	20·9	0·2349	0·0053	219·0	37·4
	AW	0·3918	0·0063	64·7	47·4	0·3660	0·0069	321·2	12·1	0·2421	0·0063	220·8	40·0
CPX	UW	0·5076	0·0233	127·8	15·2	0·3532	0·0244	3·8	64·2	0·1392	0·0316	223·6	20·4
	LW	0·4568	0·0170	130·3	20·9	0·3445	0·0159	1·4	58·6	0·1987	0·0184	229·3	22·3
	AW	0·4534	0·0194	126·6	25·2	0·3363	0·0168	1·0	51·0	0·2103	0·0184	230·9	27·6
OPX	UW	0·4545	0·0282	77·9	41·0	0·3827	0·0284	327·9	21·4	0·1628	0·0318	217·8	41·3
	LW	0·4395	0·0233	92·0	28·3	0·3768	0·0213	340·9	33·8	0·1837	0·0248	212·3	43·0
	AW	0·4694	0·0290	87·0	29·4	0·3670	0·0230	332·2	36·7	0·1636	0·0294	204·5	39·4
PP074 grain tracings													
Plag	UW	0·6819	0·0050	106·4	20·7	0·2945	0·0043	357·4	40·7	0·0236	0·0019	216·3	42·1
	LW	0·6056	0·0046	105·5	21·8	0·3395	0·0041	355·7	40·3	0·0549	0·0022	216·4	41·8
	AW	0·5976	0·0048	105·6	21·0	0·3424	0·0024	356·3	40·8	0·0600	0·0024	215·7	41·8
CPX	UW	0·6798	0·0137	108·1	19·4	0·2953	0·0114	1·2	39·5	0·0249	0·0072	218·1	44·1
	LW	0·5967	0·0113	106·4	20·1	0·3378	0·0105	359·0	39·4	0·0656	0·0049	217·0	43·8
	AW	0·5989	0·0119	106·8	19·6	0·3371	0·0052	0·2	38·8	0·0640	0·0052	217·5	44·7
OPX	UW	0·6055	0·0298	97·9	13·1	0·3852	0·0309	355·9	41·8	0·0093	0·0186	201·5	45·3
	LW	0·5206	0·0279	100·3	9·9	0·3879	0·0264	2·1	39·0	0·0914	0·0312	202·0	49·3
	AW	0·4977	0·0310	101·5	6·2	0·4196	0·0278	7·0	36·2	0·0827	0·0301	199·9	53·1
PP074 image analysis of grain boundary data													
Plag	UW	0·6297	0·0035	106·2	19·3	0·3262	0·0030	358·0	41·8	0·0441	0·0013	214·6	41·9
	LW	0·5828	0·0035	106·7	20·0	0·3499	0·0031	357·5	42·1	0·0673	0·0015	215·3	41·2
	AW	0·5875	0·0047	106·3	19·8	0·3472	0·0041	357·2	42·2	0·0653	0·0018	214·7	41·2
CPX	UW	0·6177	0·0100	105·2	18·6	0·3367	0·0083	359·0	39·7	0·0455	0·0037	214·4	44·4
	LW	0·5709	0·0088	105·5	16·8	0·3643	0·0078	359·3	42·8	0·0648	0·0040	211·5	42·4
	AW	0·5693	0·0120	104·3	16·5	0·3701	0·0110	358·5	42·5	0·0606	0·0061	210·2	42·9
OPX	UW	0·5817	0·0213	109·2	17·0	0·3541	0·0185	1·4	45·0	0·0642	0·0128	214·1	40·1
	LW	0·5169	0·0200	112·1	5·4	0·3847	0·0181	16·2	47·1	0·0985	0·0148	207·1	42·4
	AW	0·5311	0·0378	295·1	2·7	0·3931	0·0310	27·6	42·6	0·0758	0·0314	202·2	47·2
PP074 intercept-counting method													
Plag	GB	0·6694	—	83·7	35·6	0·1921	—	333·2	26·1	0·1385	—	215·9	43·1
	NGB	0·5940	—	88·9	31·2	0·2197	—	336·6	32·0	0·1863	—	212·1	42·2
CPX	GB	0·6309	—	79·3	35·9	0·2075	—	327·4	27·3	0·1616	—	209·8	41·9
	NGB	0·6144	—	91·1	31·8	0·2092	—	338·6	31·8	0·1765	—	214·8	41·9
OPX	GB	0·5447	—	91·0	24·8	0·2432	—	341·5	35·9	0·2121	—	207·4	43·9
	NGB	0·5526	—	121·8	1·1	0·2351	—	30·7	46·5	0·2123	—	212·9	43·5

Plag, plagioclase; CPX, clinopyroxene; OPX, orthopyroxene. Analysis type: UW, unweighted; LW, length-weighted; AW, area-weighted. For intercept method: GB, with grain boundaries; NGB, no grain boundaries. Eigenvalues ($g_1 > g_2 > g_3$) normalized to 1·0. For intercept-counting method, eigenvalues are for orientation matrix. Eigenvectors in geographic coordinates.

procedure and calculation of uncertainties described above are then applied to these weighted CDFs.

Our grain-tracing technique provides length information, generated by NIH Image at the same time as the orientations are measured. Additional information is required to allow area weighting. We have traced the widths of grains orthogonal to the crystallographic direction of interest and approximately at the midpoint of each

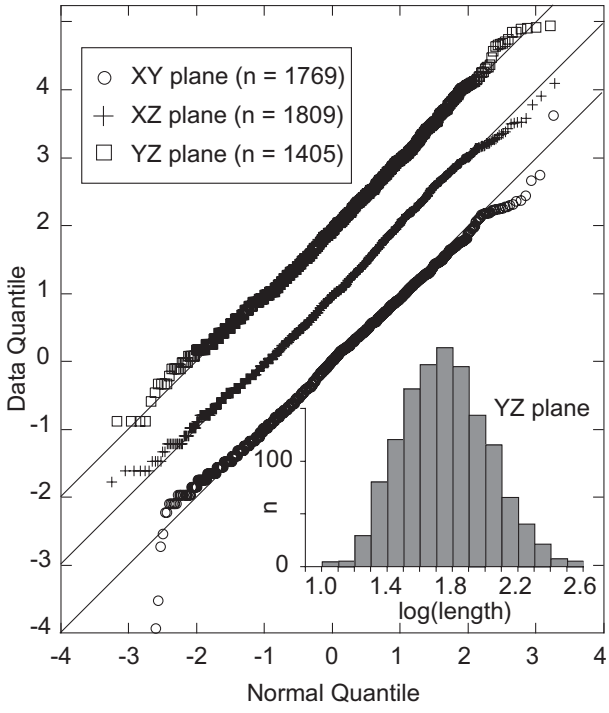

Fig. 9. Grain length distributions for sample PP046 (plagioclase *a–c* plane tracings). Lengths have an approximate log-normal distribution (inset shows example for *YZ* plane). For a log-normal distribution, the normal quantile versus data quantile should lie along the 1:1 line. Data for the *XZ* and *YZ* planes offset for clarity. Grains with log(length) values of more than 2 standard deviations from the mean are trimmed prior to calculating the best-fit strain tensor.

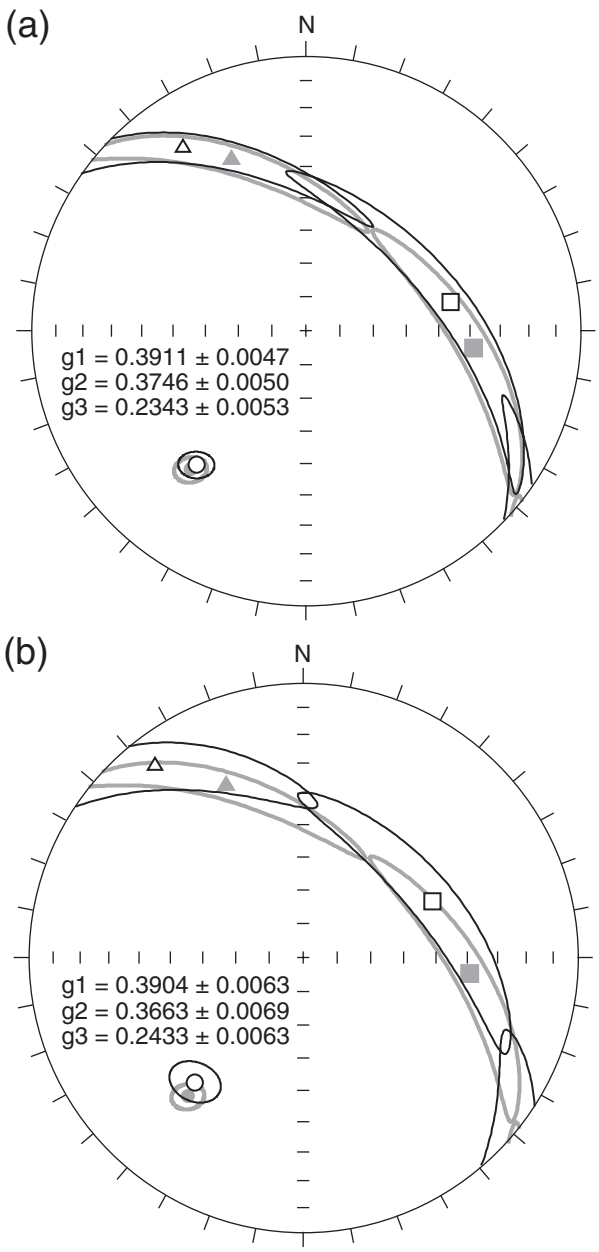

Fig. 10. Comparison of (a) length-weighted and (b) area-weighted results for sample PP046 (plagioclase *a–c* plane tracings). Principal eigenvectors (square, maximum; triangle, intermediate; circle, minimum) and associated 95% confidence bounds shown as fine black line. Mean eigenvalues and 1σ errors shown for reference. Note that the mean eigenparameters determined from the pseudosamples differ slightly from the best-fit values (Table 1). Thick dark grey line and closed symbols indicate results from the unweighted case (Fig. 8).

grain. These orthogonal tracings are then matched with the corresponding lengths and the apparent aspect ratio of the grain is calculated.

Both grain length and area are typically log-normally distributed (Fig. 9). This is most readily demonstrated on a quantile–quantile (*Q–Q*) plot that compares the probability distribution of the data with that expected from a log-normal distribution. For sample PP046, the lengths of the *a–c* plane tracings in plagioclase grains are well fitted by a log-normal distribution (i.e. the observed and predicted quantile values fall on the 1:1 line). The only significant deviations from this distribution occur at values more than 2 standard deviations from the mean. These deviations are not unexpected. For example, the number of very large grains is relatively small and we might expect that the true distribution is not necessarily well represented, even in an oversized thin section. Similarly, the smallest grains are also poorly represented because many of these grains are too small to allow tracing of a crystallographic direction (e.g. no twins may be visible in a small grain). Given the limitations of the data at both small and large sizes, we suggest that trimming the observed orientation distribution at $\pm 2\sigma$ (the standard deviation of the log-normal distribution of weights) is warranted. All weighted data shown below have been subjected to this trimming.

Length- and area-weighted results for the plagioclase fabric in sample PP046 are shown in Fig. 10. In both cases, the orientation of the foliation plane and the

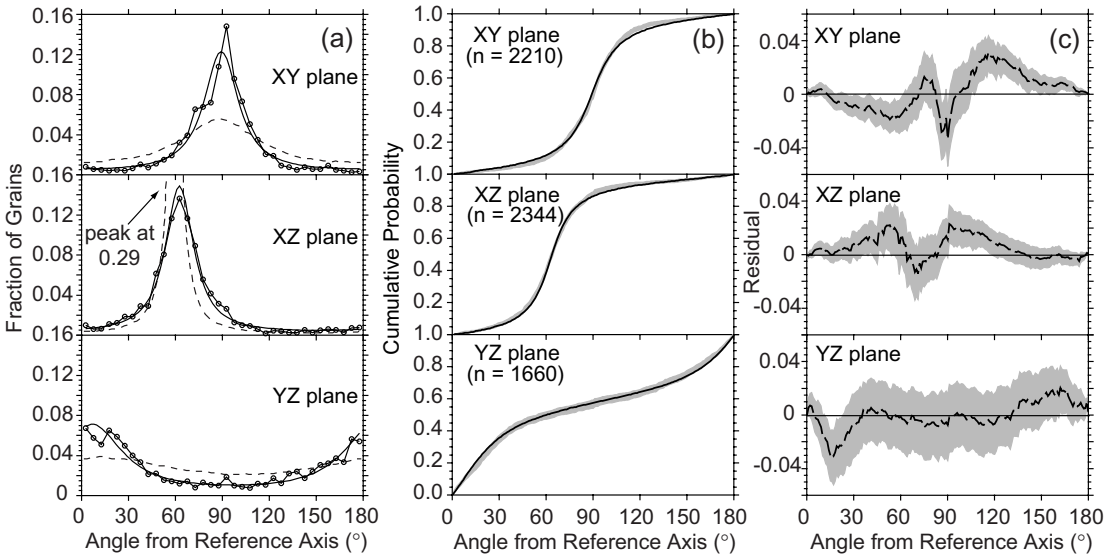

Fig. 11. Sectional data for well-foliated sample PP074 (plagioclase *a–c* planes; unweighted). (a) Comparison of original orientation data (line with circles) and orientation data predicted from best-fit tensor (line). Dashed lines show predicted orientation distribution from sectional ellipse method. Note that the curve for the sectional ellipse method results for the XZ plane has been truncated. (b) Cumulative distribution functions (CDFs) for each section. The grey band indicates the 95% bounds on the CDFs of 500 pseudosamples drawn from the original data. Black line indicates the CDF produced by the best-fit strain tensor. (c) Residuals (data – model) for each section. Thin dashed line (grey band) indicates the mean (95% bounds) of the residual.

lineation within that plane differ slightly from the unweighted case (Fig. 8). The resulting orientation ellipsoids are less anisotropic than for the unweighted case (Table 1)—apparently at odds with our expectation that larger grains are, probably, better aligned. The lower degree of anisotropy for the weighted cases reflects the fact that the grains are being treated as true passive markers (i.e. their lengths as well as their orientations change when deformed). Under these conditions, a less anisotropic strain tensor is required to produce the same orientation matrix. Although this result is perhaps not desirable in terms of our expectations, we note that the degree of anisotropy inferred from our fabric description is, at some level, arbitrary, as the crystal alignment probably did not result by the physical process (strain of an initially uniform distribution) used in the modeling. Moreover, our treatment of the length-weighted case ensures that both the unweighted and length-weighted analyses accurately recover an imposed strain tensor (see the Appendix). Thus, the method is ideally suited for strain analysis of passive markers, both when treated as unit vectors and when length information is retained. In principle, area weighting should provide a fabric estimate that most nearly reflects the true volume fabric of the sample. Indeed, as we will see below, the eigenvalues for the weighted cases more closely match those derived from EBSD measurements. In most cases, length weighting provides similar results to those obtained by area weighting (Table 1). As the former requires no additional tracing data, we suggest that length-weighted data could be used routinely to provide an improved estimate of the sample volume fabric (relative to the unweighted analysis).

Fabric results for well-foliated sample (PP074)

The results described above for sample PP046 using the CDF method are similar to those obtained with the sectional ellipse method. In contrast, sample PP074 has a very pronounced fabric that proved problematic for the sectional ellipse method. Specifically, combining the sectional ellipse data for this sample resulted in fabric hyperboloids (one negative eigenvalue) and very poor fits to the observed sectional orientation data. The hyperboloids resulting from such samples have commonly been taken as evidence that the data were flawed (De Paor, 1990; Robin, 2002). In this section, we demonstrate that the CDF method can provide a close match to the observed sectional orientation data, even for samples with extreme fabrics.

Angular orientation histograms for sample PP074 (Fig. 11a) illustrate the strong foliation of this sample. Angular data (binned at 5°) for both the XY and XZ planes are characterized by maxima that are approximately 25 times greater than the minimum values. Moreover, the histograms for these sections deviate from simple unimodal distributions. The XY histogram has a narrow peak at ~90° and a significant shoulder near 75°. A small shoulder is also evident (at ~90°) in the

histogram for the XZ section and the fraction of grains with orientations >100° is near zero. The sectional ellipse technique yields a poor fit to these data (Fig. 11a). The anisotropy of the XY and YZ planes is significantly underestimated. The predicted distribution of orientations in the XZ plane has a maximum that is offset from and approximately 2·5 times the observed peak height, presumably reflecting the influence of the very low fraction of grains away from the peak. Although minor improvements in the fit may be achieved by allowing rotations of each sectional ellipse, the overall fit produced by the sectional ellipse technique is quite poor.

In contrast, the CDF method provides a much closer match to the histograms for all three sections (Fig. 11a), though the second-rank symmetric tensor solution from this method also cannot fit the shoulders on the XY and XZ orientation distributions. This minor misfit is also evident in the predicted and observed CDFs (Fig. 11b). For both the XY and XZ planes, the CDF predicted from the best-fit strain tensor matches the steepest portion of the data CDF (corresponding to the histogram peak) but, in other intervals, sometimes lies outside of the 95% confidence bounds for the original data. Deviations of the sectional orientation data from a unimodal distribution (corresponding to a second-rank symmetric tensor) are most clearly seen in the pattern of residuals (Fig. 11c). For the XY plane, the best-fit strain tensor yields statistically significant positive residuals over a broad range of angles >100°. This mismatch reflects the compromise solution necessary to accommodate the distinct shoulder near 70° in the original data. Similarly, the positive residuals in the XZ plane match closely the location of the shoulder at 90° in the histogram data. These statistically significant misfits in the XY and XZ planes could be used to construct a higher-order solution for the fabric of this sample.

Analysis of the unweighted plagioclase *a*–*c* plane orientations for sample PP074 gives a distinctly tri-axial orientation ellipsoid (Table 1). All three eigenvalues are statistically distinct and the 95% confidence ellipses on the eigenvectors are remarkably small (<2·5° for all semi-axes). Both length- and area-weighted analyses for sample PP074 (Table 1) yield essentially identical eigenvectors as for the unweighted case. Although the angular orientation distributions for the weighted cases (Fig. 12) are generally similar to the unweighted case, the peaks of the weighted XY and XZ histograms are higher relative to the troughs (>100:1) than with the unweighted data (~25:1). As noted for PP046, the eigenvalues for the weighted cases indicate a lower degree of anisotropy than for the unweighted case. The results for sample PP074 illustrate that the CDF method provides a reasonable fit to data from samples with extremely well-developed fabrics that might otherwise be unsuitable for analysis with the sectional ellipse technique.

DISCUSSION

The CDF method provides a robust way of determining the 3D fabric (or strain) ellipsoid from orientation data on orthogonal sections. When applied to traces of crystallographic features, we suggest that the resulting fabric approximates the LPO. We begin our discussion by examining the validity of this assertion and some limitations of the crystallographic fabric reconstructed from tracings of crystallographic features. We then examine the homogeneity of the sample fabrics, comparing results from our over-sized thin sections with those obtained using smaller areas. Next, we compare the LPO and SPO fabrics, as this comparison sheds light on the mechanism of fabric development. The discussion concludes with a comparison of the silicate fabrics with proxy fabric measurements using magnetic anisotropy.

Validity of crystallographic data obtained from grain-tracing method

Our grain-tracing technique is based on identifying the projections of crystallographic features on three orthogonal sections and, therefore, should yield crystallographic fabrics. For orthopyroxene and clinopyroxene, the projection of the *c*-axis is traced and, hence, the 3D fabric ellipsoid should reflect the preferred orientation of the crystallographic *c*-axis. For plagioclase *a*–*c* fabrics, the significance of the eigenvector associated with the maximum eigenvalue of the fabric ellipsoid is less obvious. Two lines of evidence, outlined below, suggest that the maximum of the plagioclase *a*–*c* fabric may approximate the preferred orientation of the crystallographic *c*-axis.

Comparison of plagioclase *a*–*c* fabrics and pyroxene fabrics from the same sample provides qualitative support for the crystallographic significance of the maximum in the plagioclase fabric (Fig. 13). For this comparison, we have used length-weighted results for all phases; unweighted or area-weighted results (Table 1) give similar answers. For sample PP046, both the clinopyroxene and orthopyroxene fabrics have maxima near that determined for the plagioclase *a*–*c* fabric (Fig. 13a). Although the orthopyroxene fabric is based on a small number of grains (average of 64 per section) and, hence, has large associated uncertainties, all three eigenvectors for the orthopyroxene fabric are statistically indistinguishable from those of the plagioclase fabric. The clinopyroxene fabric (based on an average of 182 grains per section) is distinct from the plagioclase fabric, although the south-easterly orientation of the clinopyroxene maximum is broadly compatible with that of the plagioclase fabric. Pyroxene fabrics from sample PP074 corroborate the well defined tri-axial fabric of plagioclase *a*–*c* planes (Fig. 13b). The clinopyroxene fabric is essentially identical to that of the plagioclase, both in direction and

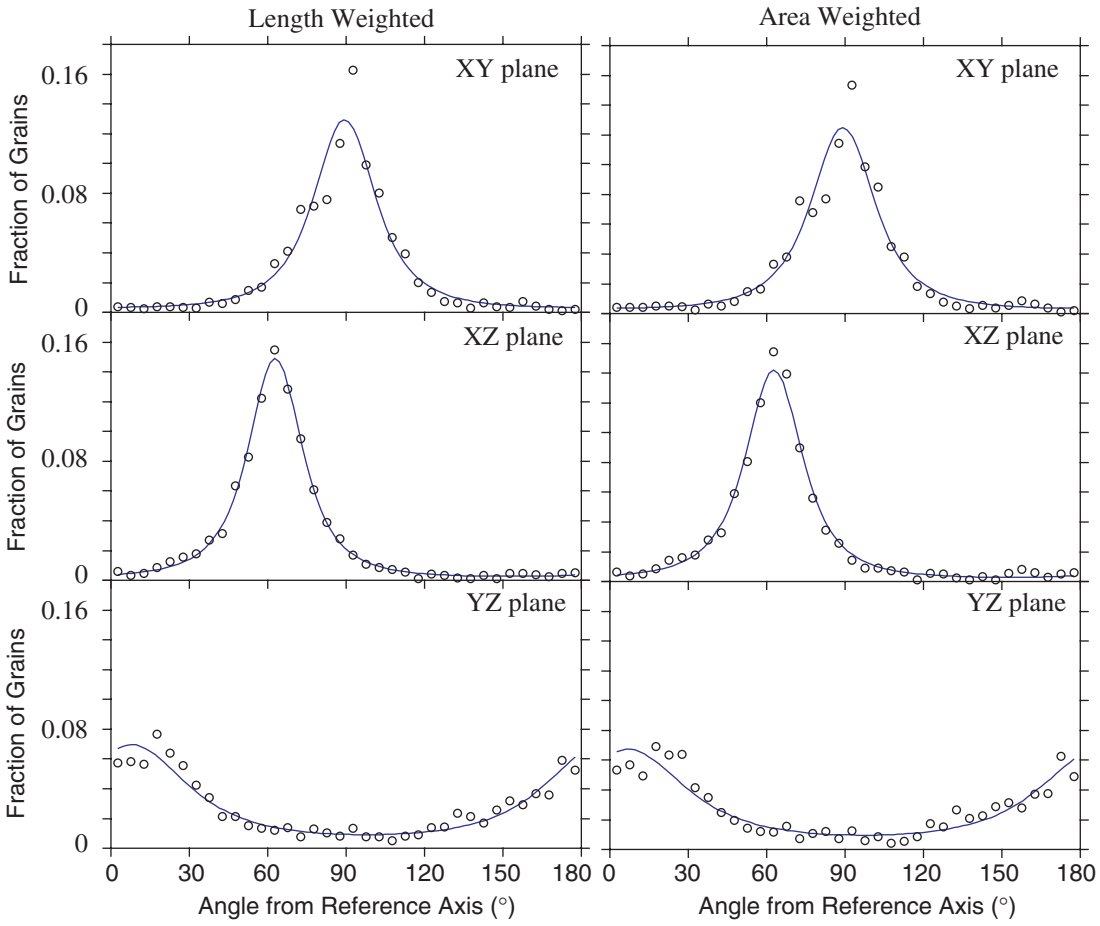

Fig. 12. Comparison of length-weighted and area-weighted results for sample PP074 (plagioclase *a–c* plane tracings). Weighted angular orientation distribution shown by circles. Orientation distribution predicted from best-fit tensor shown by line. Although the overall distributions are similar to the unweighted case (Fig. 10a), the peak values are somewhat higher and the lowest values for the weighted cases are much closer to zero. Original data were binned at 5° intervals. Distribution trimmed at $\pm 2\sigma$, as described in text.

magnitude of anisotropy (Table 1). The orthopyroxene fabric (based on an average of 49 grains per section) is more poorly defined, but, nonetheless, yields a maximum eigenvector that is quite similar to that of the plagioclase fabric.

EBSD results from sample PP074 provide more direct support for the crystallographic significance of the fabrics derived from our grain-tracing technique (Fig. 14). EBSD allows crystallographic orientation data to be generated quickly and efficiently, by detecting and indexing diffraction patterns produced by back-scattered electrons (Prior *et al.*, 1999). Crystallographic data were obtained on a 0·25 mm grid for a standard-sized thin section (~20 mm × 40 mm), yielding 6963 indexed patterns for plagioclase and 861 for clinopyroxene. The mean orientations of crystallographic axes or poles to planes (Table 2) were determined from eigenvalue analysis of the corresponding orientation matrix and error estimates were determined using the bootstrap technique described above. The evenly spaced grid for the EBSD data effectively yields an area-weighted mean orientation that is suitable for comparison with the area-weighted results from grain tracings. The bootstrap error estimates for the EBSD data, however, underestimate the true variability, as each grid point is treated as an independent grain during the resampling procedure.

The orientations of crystallographic features defined by EBSD generally agree with those inferred from the grain-tracing technique. Our grain-tracing technique defines a plagioclase fabric ellipsoid, the minimum eigenvector of which corresponds to the pole to the silicate foliation plane. As expected, poles to plagioclase {010} planes measured by EBSD (Fig. 14a) are tightly clustered about this same direction (within about 2°). Although more scattered, the distribution of plagioclase *c*-axes determined by EBSD data also reveals a weak lineation (Fig. 14b) in a direction that is generally consistent with the maximum orientation defined by the grain-tracing

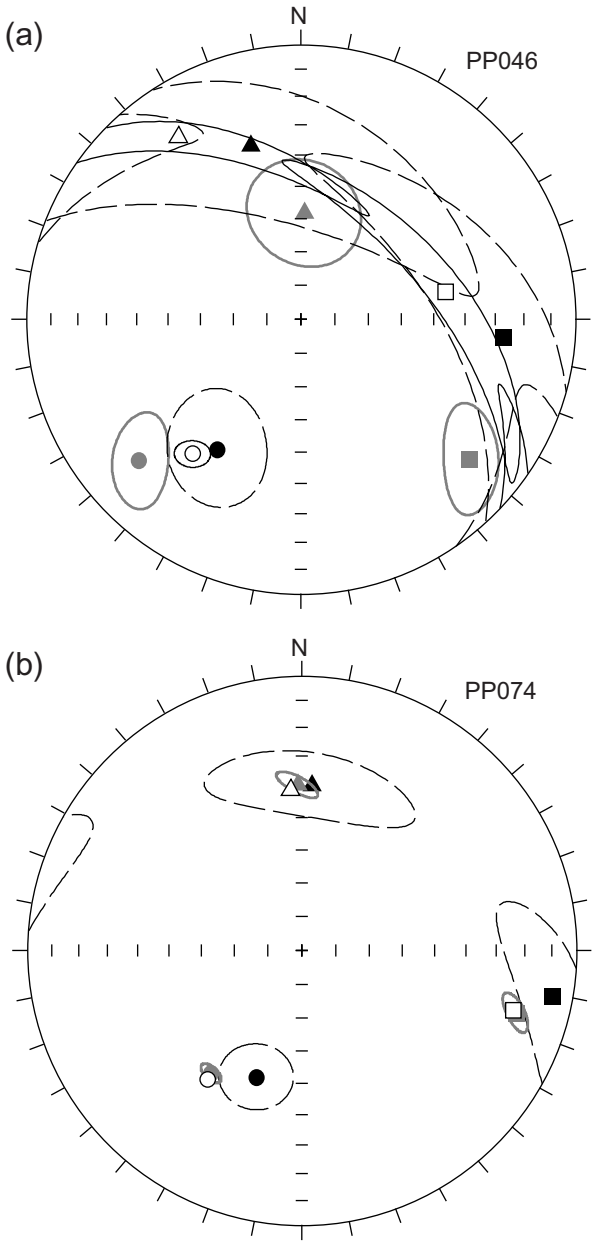

Fig. 13. Comparison of length-weighted fabrics from mineral phases in samples PP046 and PP074. Plagioclase results shown by open symbols and continuous lines; clinopyroxene (grey); orthopyroxene (black with dashed 95% confidence bounds). Square, maximum; triangle, intermediate; circle, minimum.

technique (Fig. 13b; recall that, in tracing the *a*–*c* plane for plagioclase, we assume that the long dimension in this plane coincides with the *c*-axis). Though determined from a smaller number of grains, the distribution of clinopyroxene *c*-axes from EBSD yields a mean orientation (Fig. 14c) that is very similar to that determined from the grain tracings.

Direct comparison of the degree of preferred orientation in the EBSD and grain-tracing results is more problematic. A separate eigenparameter characterization is required for each crystallographic axis or pole distribution and it is not clear how these various crystallographic fabric estimates should be combined for direct comparison with the grain-tracing LPO. The *c*-axis fabric estimated from EBSD should be most comparable with the area-weighted clinopyroxene grain-tracing results. The EBSD clinopyroxene *c*-axis fabric is somewhat less anisotropic (maximum/minimum eigenvalue ratio, $P = 5{\cdot}5$) and has a weaker lineation (maximum/intermediate eigenvalue ratio, $L = 1{\cdot}3$) than for the grain-tracing fabric ($P = 9{\cdot}3$, $L = 1{\cdot}8$). Poles to {100} for clinopyroxene, which best reflects the degree of foliation, indicate a stronger anisotropy ($P = 7{\cdot}6$), more comparable with the grain-tracing fabric. For plagioclase, the distribution of poles to {010} should most closely reflect the *a*–*c* plane-tracing fabric. The {010} fabric reveals a pronounced anisotropy ($P = 9{\cdot}5$)—nearly identical to that from the grain tracings ($P = 10{\cdot}0$). However, the plagioclase *c*-axis fabric determined by EBSD reveals a much weaker lineation ($L = 1{\cdot}1$) than that inferred from the grain tracing ($L = 1{\cdot}7$).

Overall, the EBSD data provide strong support for the crystallographic significance of the grain tracings, as the directions and degree of anisotropy from both techniques closely agree. However, the degree of lineation within the foliation plane is systematically higher in the grain-tracing results. This discrepancy is larger for the plagioclase *a*–*c* plane tracings than for clinopyroxene. Albite twinning would tend to reduce the degree of anisotropy in the EBSD plagioclase fabric, but this effect is relatively minor and could not account for the significant differences in the degree of lineation for the EBSD and tracing fabrics. The discrepancy in the degree of lineation for plagioclase may reflect a limitation of the tracing technique. For example, for grains with sub-equal dimensions parallel to the crystallographic *c*- and *a*-axes, the tracings of the *a*–*c* plane will provide a poor estimate of the true *c*-axis orientation. Conversely, the more pronounced plagioclase (and, to some degree, clinopyroxene) lineations in the tracing data may reflect a significant contribution from the SPO fabric in the grain-tracing results (see below).

Evaluation of fabric homogeneity

The fabric results described above were based on the analysis of a large number of grain tracings from oversized thin sections. Frequently, only a small number of orientation data may be available, either because a standard-sized thin section (approximately one-third of the area of our sections) is used or because the average grain size is large. Moreover, the fabric within a block sample

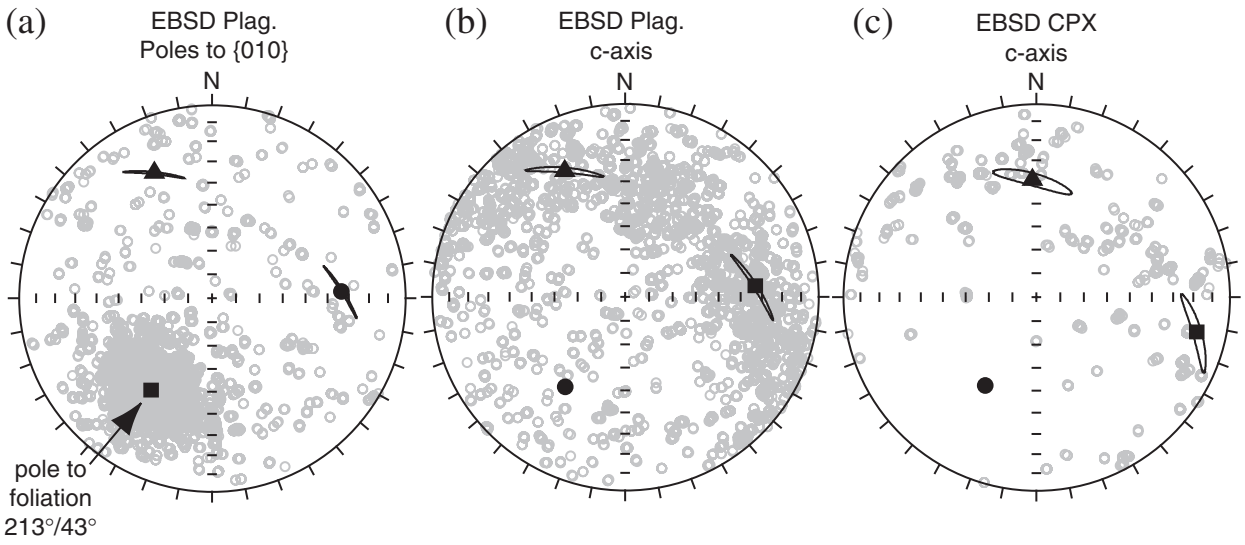

Fig. 14. EBSD crystallographic data for sample PP074. (a) Poles to the {010} plane for plagioclase ($n = 6962$). The maximum concentration corresponds within 2° to the pole to foliation determined from the grain tracings. Individual poles shown as grey circles. Mean eigenvector orientations (square, maximum; triangle, intermediate; circle, minimum) and 95% confidence bounds determined by same bootstrap resampling method as for grain tracings. (b) Crystallographic *c*-axis distribution for plagioclase. (c) Crystallographic *c*-axis distribution for clinopyroxene ($n = 860$). The maximum concentration is indistinguishable from the *c*-axis orientation inferred from grain tracings. All plots are lower-hemisphere equal area projections.

Table 2: Summary of EBSD results for sample PP074

Phase	Type	g_1	1σ	Dec	Inc	g_2	1σ	Dec	Inc	g_3	1σ	Dec	Inc
Plag	*a*-axis	0·4941	0·0039	336·5	31·2	0·4548	0·0040	89·8	33·2	0·0511	0·0012	214·6	41·1
	{100}	0·4804	0·0036	337·5	31·5	0·4609	0·0036	90·2	32·1	0·0587	0·0012	214·3	41·8
	b-axis	0·8082	0·0031	214·3	42·8	0·1055	0·0021	330·1	25·2	0·0863	0·0018	80·7	36·7
	{010}	0·8134	0·0031	214·1	42·7	0·1011	0·0022	335·0	29·1	0·0855	0·0019	86·6	33·5
	c-axis	0·4539	0·0039	84·9	33·4	0·4168	0·0038	334·4	27·9	0·1293	0·0027	214·0	43·7
	{001}	0·4589	0·0040	85·3	32·1	0·4012	0·0038	336·1	27·6	0·1399	0·0027	214·4	45·2
CPX	*a*-axis	0·7056	0·0104	216·0	46·0	0·1729	0·0077	113·0	12·2	0·1221	0·0049	12·0	41·4
	{100}	0·7422	0·0112	214·6	44·5	0·1604	0·0083	110·1	14·3	0·0974	0·0044	6·8	42·0
	b-axis	0·5011	0·0106	1·1	41·0	0·3379	0·0097	112·8	23·1	0·1610	0·0082	223·9	40·2
	{010}	0·5011	0·0115	1·1	41·0	0·3379	0·0090	112·8	23·1	0·1610	0·0090	223·9	40·2
	c-axis	0·5073	0·0115	102·1	16·6	0·4010	0·0105	358·2	38·8	0·0918	0·0050	210·4	46·5
	{001}	0·4962	0·0105	101·0	17·2	0·3766	0·0102	358·7	34·3	0·1272	0·0058	213·0	50·4

Plag, plagioclase; CPX, clinopyroxene. Eigenvalues ($g_1 > g_2 > g_3$) normalized to 1·0. Eigenvectors in geographic coordinates.

may be heterogeneous at the scale of a thin section or over the volume enclosed by the orthogonal sections.

In order to evaluate the fabric homogeneity, as well as the number of grain orientations required to characterize a particular petrofabric, we have found it useful to examine 3D fabrics generated from subsets of the original data (Fig. 15). The coordinates of each orientation observation are used to subdivide the data from each oversized section into three subsets, each approximately the size of a standard thin section. The CDFs are calculated for each of these nine subsets (Fig. 15a) and then a separate 3D fabric estimate is made for each of the 27 permutations of these subsets (Fig. 15b). For samples such as PP046, with weakly developed fabrics, the resulting 3D fabrics exhibit substantial variability. The eigenvectors from most of these permutations are generally compatible with the 95% confidence bounds determined from the full data set, providing another illustration of the uncertainty in

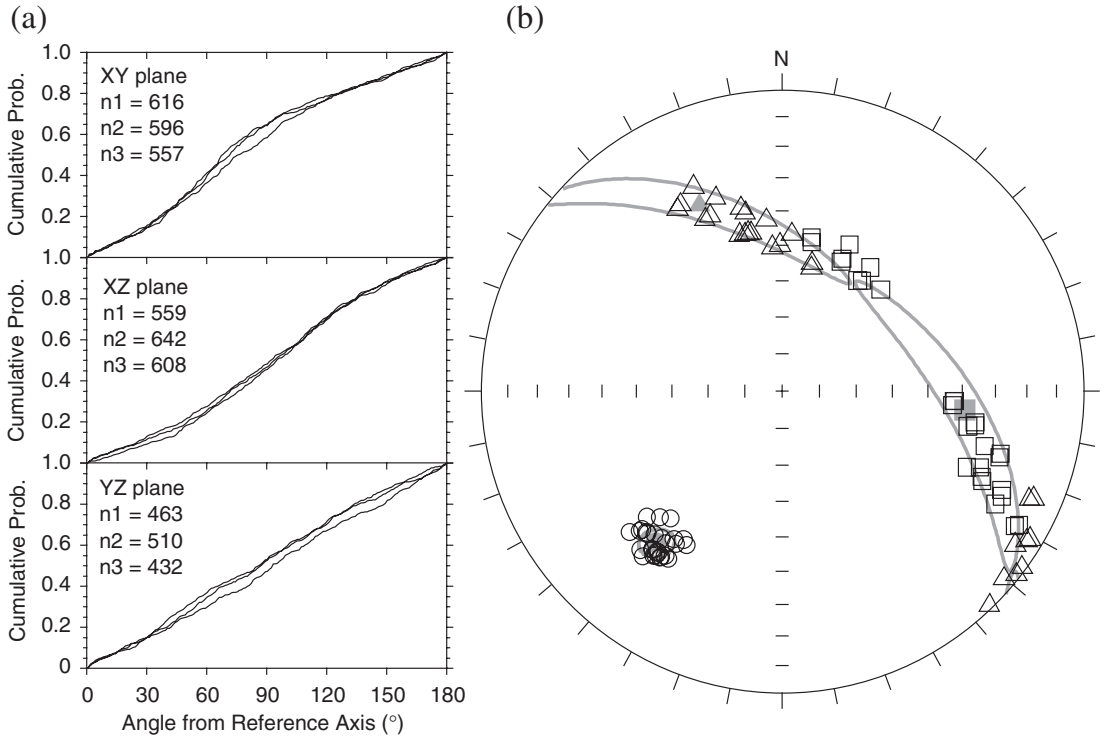

Fig. 15. Fabric variability within sample PP046 (plagioclase *a–c* tracing; unweighted). Grain orientations from each oversized thin section were subdivided into three sections, each nominally the size of a standard thin section. (a) Cumulative distribution functions for each subsection. (b) Lower-hemisphere equal area plot showing the eigenvectors of the 27 permutations formed by using one subsection from each of the three planes (square, maximum; triangle, intermediate; circle, minimum). Mean fabric tensor and 95% confidence ellipses (heavy grey lines and symbols) from Fig. 8 shown for reference.

fabric estimates from these samples. For samples with weak to moderate fabrics, results based on the smaller number of grains (~500) from a standard-sized thin section would be associated with very large errors and should be viewed with caution. In contrast, the 27 subfabrics from well-foliated sample PP074 are well clustered and similar to the fabric estimated from the full data set, indicating that standard-sized thin sections may yield robust fabric data for samples with strong fabrics.

The validity of any fabric characterization will depend upon the number of grains analyzed (a function of grain size, modal percentage and thin section area), as well as the degree of fabric development. To illustrate these effects for our two test samples, we generated a subset of each orthogonal section by randomly selecting a square region representing some fraction of the total thin section area. The orientation data from these subsets were then analyzed (using area weighting) to yield the best-fit fabric ellipsoid. One hundred such pseudosamples were generated and the angular deviation of each eigenvector was calculated relative to the mean eigenvectors determined using the entire data set. For the plagioclase fabric of sample PP046, the minimum eigenvector is relatively well determined for an area corresponding to a standard-sized thin section (maximum angular deviation ~15°; Fig. 16a). In contrast, little reliable information on the maximum eigenvector could be obtained with the smaller number of grains on a standard-sized thin section. We note that the angular deviations for all eigenvectors are relatively stable at fractional areas of greater than about 0·5, suggesting that the plagioclase fabric may be reasonably well represented by the full data set. As expected from the smaller number of clinopyroxene grains, significant angular deviations are possible for fractional areas of as high as 0·7 (Fig. 16b), suggesting that even the oversized thin section may not adequately represent the clinopyroxene fabric. The pronounced foliation in sample PP074, however, is well approximated over a wide range of fractional areas (Fig. 16c and d). Because the number of grains is comparable with that in sample PP046, this robustness must be attributed to the degree of fabric development.

Comparison of shape- and lattice-preferred orientations

During the development of fabrics produced by deposition of crystals from density currents or plumes, the shapes

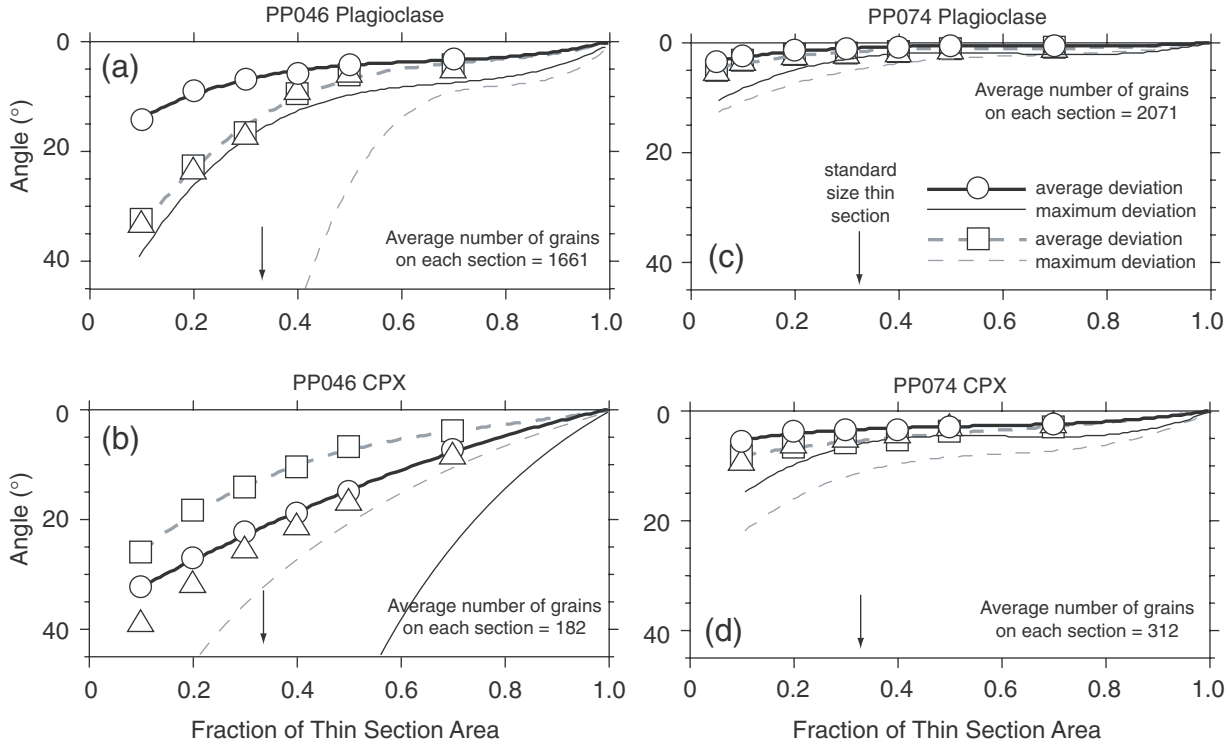

Fig. 16. Fabric variability in samples PP046 and PP074 as a function of the thin section area analyzed. Upper panels illustrate average (heavy lines with symbols) and maximum (finer lines) deviation of eigenvectors from the mean determined from the full plagioclase data set from the oversized thin section as a function of the fractional area of the thin section used for the analysis. Square, maximum; triangle, intermediate; circle, minimum. Bounds on intermediate eigenvectors are similar to those for maximum (a, c and d) or minimum (b) eigenvector and are omitted for clarity. Arrow indicates approximate size of standard thin section. All results shown are for area-weighted analysis.

of the grains will determine the character and extent of fabric development (Fernandez, 1987; Hunter, 1987, 1996; McBirney & Nicolas, 1997). Likewise, during the early stages of compaction or when slumping of an unconsolidated crystal mush takes place, the shapes of the grains will govern the fabric development (Ildefonse *et al.*, 1992; Meurer & Boudreau, 1998*b*). However, because the grains involved in these processes are mostly euhedral, their shapes are governed by their crystallography and so the LPOs should be coincident with the SPOs during the early stages of cumulate formation. It is only during solid-state recrystallization, or low liquid fraction crystallization, that the LPO and SPO fabrics of rocks will differ. Thus, comparison of the LPO and SPO fabrics may provide valuable information on the primary processes of cumulate formation. Standard image analysis techniques for SPO analysis of thin sections require complete grain boundary digitization, which is difficult to automate and extremely time-consuming. For comparison with the LPO fabrics described above, we have digitized the grain boundaries for all three sections of PP074 (Fig. 17a). The images obtained with plane- and cross-polarized light used for the grain tracings were used in a graphics program to digitize the grain boundaries using a polygon tool. This process required about 45 hours per section for digitization and error checking, and so is not a viable method for fabric analysis. The digitized images were then analyzed in NIH Image to determine the area, long axis length and direction, and the center of mass of each grain.

Comparison of the grain-tracing LPO (from traces of crystallographic features) and SPO fabrics (from analysis of grain boundaries) for plagioclase, clinopyroxene and orthopyroxene for PP074 shows them to be remarkably similar (Fig. 18a and b). Both fabrics are statistically triaxial, with very similar eigenvectors as well as eigenvalues (Table 1). Slight differences in the eigenvectors and eigenvalues of the SPO fabric relative to the grain-tracing LPO fabric are evident for both clinopyroxene and orthopyroxene. These differences probably reflect the automated method by which the orientation and lengths of the long axes are defined in NIH Image. For subequant rectangular grains, the long axis for an SPO analysis is along a diagonal. This effect is evident, particularly for orthopyroxene, in rectangular reconstructions of the grain-tracing LPO and SPO fabrics (Fig. 17b and c). The large size and sub- to euhedral shape of the orthopyroxene grains indicate they accumulated early in the formation of these cumulates. The blocky shape of the

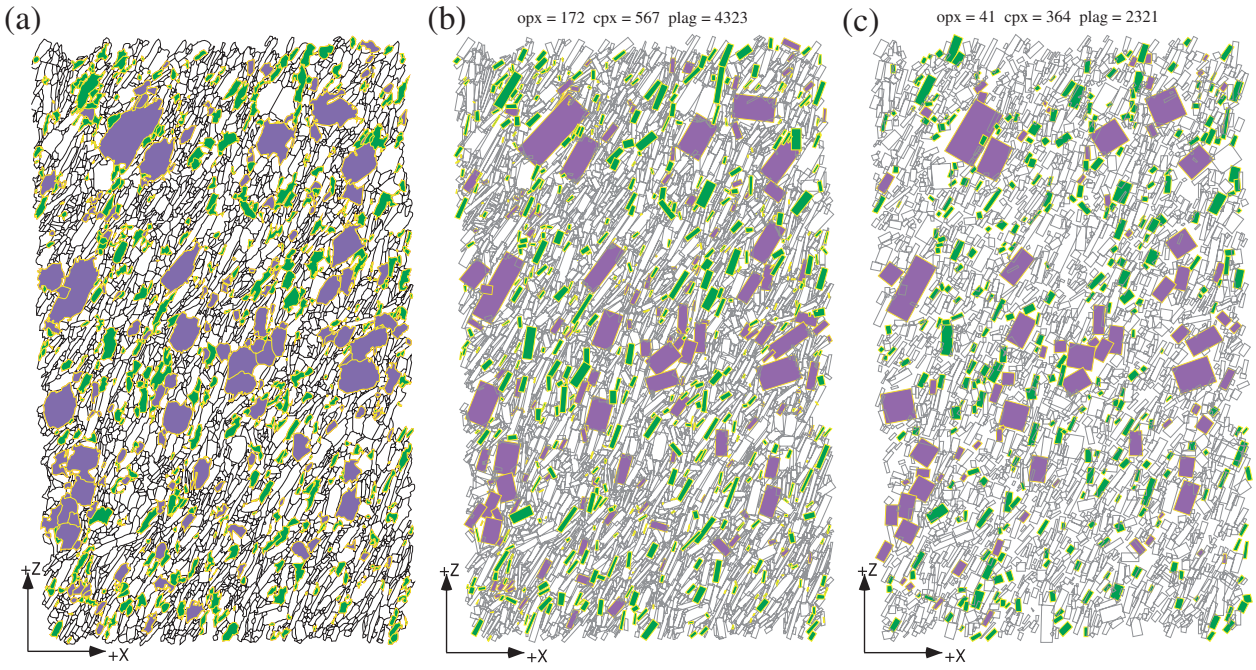

Fig. 17. Grain boundary tracings and rectangular reconstructions for sample PP074 (XZ section). (a) Digitized grain boundary data. Only grains completely within the thin section were traced. (b) Rectangular reconstruction of the grain boundary data in (a) based on the area and maximum dimension of grains determined by image analysis. (c) Rectangular reconstruction based on grain tracings. Purple, orthopyroxene; green, clinopyroxene; white, plagioclase.

orthopyroxene grains probably allowed interstitial liquid to concentrate at their ends during the fabric-forming deformation by compaction and/or shearing, in a manner analogous to pressure shadows in metamorphic rocks. It is possible to discern a small rotation of the axis of the orthopyroxene into the foliation direction for the SPO fabric (e.g. large grain in upper left corner of Fig. 17b) that reflects the locations of the overgrowths, implying that they grew during the fabric-forming event (and indicating that some component of shear was involved). Crystallization of overgrowths on the cumulus orthopyroxene grains produced an SPO long-axis trace that is significantly longer than the *c*-axis trace (Fig. 17b and c). Such overgrowths enhance differences between the grain length and orientation determined in the automated analysis and the grain tracings.

The overall similarity of the orientations of the grain-tracing LPO and SPO fabrics derived from the CDF analysis might be interpreted as indicating that the fabric was primarily imparted by magmatic processes, operating at reasonably high liquid fractions. This interpretation is supported by the lack of any deformation twinning in the plagioclase, despite the fact that bent and broken grains clearly indicate that it was strained (but strained at high temperatures). The minimum eigenvalues of the plagioclase {010} fabric and plagioclase *a*–*c* plane fabric (∼0·08 and 0·06, respectively) both document a pronounced foliation. However, as noted above, there is a significant difference in the degree of lineation of the LPO fabrics from EBSD and grain tracing. Although direct comparison of the magnitude of these two fabrics is difficult, the magnitude of the grain-tracing LPO may be influenced by the aspect ratio of grains or may incorporate some component of the SPO. In addition, the assumption that the long dimension within the *a*–*c* plane coincides with the *c*-axis might not be valid. If we regard the less lineated EBSD fabric as more representative of the true LPO, then some degree of decoupling between the shape- and lattice-preferred fabrics is required. We suggest that the stronger lineation revealed in the grain tracings may reflect continued crystal growth within the foliation plane (with a low degree of melt remaining) that accentuates the shape fabric relative to the LPO.

The rectangular fabric reconstructions (Fig. 17b and c) are easily produced from the basic orientation data and some estimate of the mean aspect ratio of the grains (e.g. a constant aspect ratio or some function of the grain length). We have found them to be particularly valuable for examining mineral clustering, spatial distributions and size/orientation spatial relations. Especially valuable in this regard is the ability to display only a given mineral, or even subpopulations of minerals, based on size and orientation. This greatly simplifies the visual information

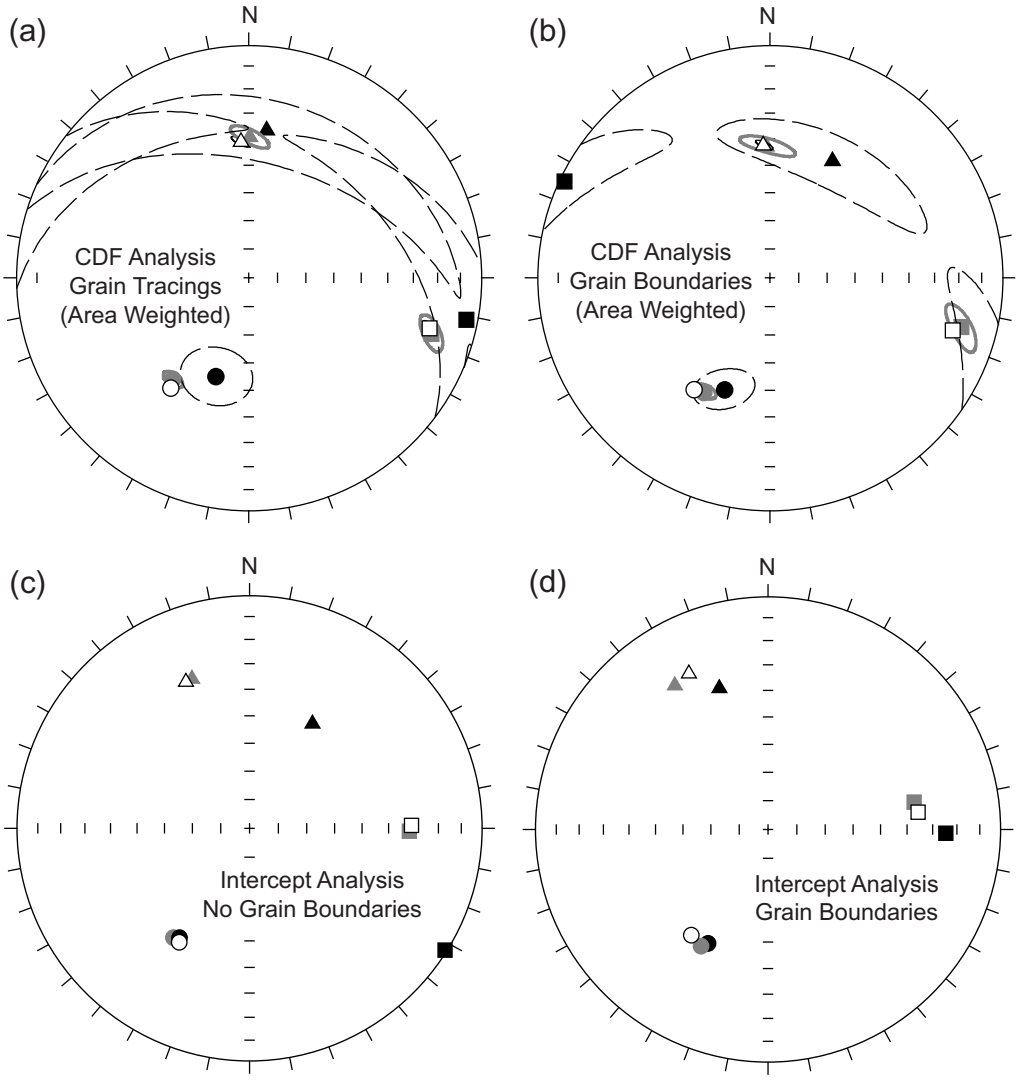

Fig. 18. Comparison of LPO and SPO for sample PP074. (a) Results from area-weighted analysis of grain-tracing data. (b) Results for area-weighted analysis of reconstructed rectangular grains (Fig. 17b) from digitized grain boundaries (Fig. 17a). (c) Results from intercept analysis method of Launeau & Cruden (1998) for the digitized grains. (d) Same as (c) but including grain boundaries. Plagioclase results shown by open symbols and continuous lines; clinopyroxene (grey); orthopyroxene (black with dashed 95% confidence bounds). Square, maximum; triangle, intermediate; circle, minimum.

provided by a cross-polarized image and allows pattern recognition.

An alternative method to determine the SPO fabric is the intercept-counting technique (Launeau *et al.*, 1990; Launeau & Robin, 1996; Launeau & Cruden, 1998). In this method, multispectral analysis of scanned images is first used to characterize the color of each mineral phase and to classify each pixel in the image. Because individual grains are typically not distinguished by such image analysis, the shape anisotropy of the sample is determined from the angular distribution of intercepts, the minimum count direction corresponding to the elongation direction of the phase boundaries. Using the software provided by P.-Y. Robin (http://www.geology.utoronto.ca/software/intercepts.html), we have applied this technique to sample PP074, both with and without the digitized grain boundaries (as in Fig. 17a). The 3D fabric was calculated from the 2D ellipse data using the method of Launeau & Cruden (1998). Because the sectional ellipse technique yields a 3D fabric that approximates the strain tensor, we have calculated the eigenparameters of the corresponding orientation matrix (Table 1) to allow more direct comparison with the results from our CDF method.

The intercept-counting technique yields eigenvectors that are broadly similar to those determined for the SPO fabric using the CDF method (Fig. 18). In particular, the

minima (poles to the foliation) are essentially identical to those determined from the CDF technique. Eigenvectors for the plagioclase and clinopyroxene fabrics are little affected by whether grain boundary data are included in the analysis. The orientations of the maximum and intermediate eigenvectors for the orthopyroxene fabric, however, are sensitive to inclusion of the grain boundary data. This presumably reflects the fact the orthopyroxene tends to occur in clumps, with grain interstices also occupied by orthopyroxene (Fig. 17a). The SPO fabrics obtained by the intercept-counting technique are significantly less anisotropic than those determined from the CDF method (Table 1). For example, the ratio of maximum to minimum eigenvalues for plagioclase (4·83 and 3·19, with and without grain boundaries, respectively) indicates a much lower degree of anisotropy than that inferred from the CDF method ($P = 9{\cdot}0$ for area-weighted case). The fabric shapes from the intercept-counting technique are also significantly more prolate than the strongly oblate SPO fabrics recovered from the CDF method. Although the intercept-counting method offers a rapid (if grain boundaries are not digitized) method for obtaining the fabric orientation, the significance of the eigenvalues in characterizing the degree of anisotropy is uncertain.

Comparison of silicate and magnetic fabrics

The techniques outlined above constitute the most direct means for estimating the 3D silicate fabric. However, the substantial amount of time required for these analyses makes it attractive to seek more rapid proxy estimates of the silicate fabric. We have examined the anisotropy of magnetic susceptibility (AMS) and the anisotropy of anhysteretic remanent magnetization (AARM; McCabe *et al.*, 1985) as possible indirect measures of the silicate fabric. Both tensors were determined from 15 measurements, using the rotatable design of Hext (1963). These magnetic methods have the advantage of providing direct 3D fabric information, having precision to detect small degrees ($\sim$0·5%) of anisotropy, and being rapid enough to collect fabric data from a large number of samples.

In samples containing magnetite (or other phases with high ferromagnetic susceptibilities), the AMS ellipsoid is commonly interpreted in terms of the statistical alignment of magnetite long axes (e.g. Uyeda *et al.*, 1963) or the anisotropic distribution of (possibly) equant grains (Hargraves *et al.*, 1991; Stephenson, 1994) imposed by a pre-existing silicate fabric. However, most mafic cumulates from the Stillwater complex lack magnetite, except for trace amounts that are exsolved from the cumulus minerals, and so its orientation is crystallographically controlled by and is closely linked to the silicate fabrics (e.g. Xu *et al.*, 1997; Selkin *et al.*, 2000). In particular, both orthopyroxene and clinopyroxene from the Stillwater complex have magnetite grains elongated (sub)parallel to the crystallographic *c*-axis, so that the AMS contribution from pyroxenes should be closely related to the pyroxene *c*-axis (Lagroix & Borradaile, 2000; Selkin *et al.*, 2003). The amount of magnetite in plagioclase is much lower and its crystallographic orientation is more variable. These results suggest that AMS should provide a reliable estimate of both the silicate fabric foliation and any lineation for samples comprising plagioclase, orthopyroxene and clinopyroxene.

The orientation of AMS fabrics from samples PP046 and PP074 generally agrees well with the silicate fabrics derived from the CDF method (Fig. 19). Individual minicore samples ($\sim$12 cm^3 volume) show some variability, but the mean eigenvectors (derived from bootstrap resampling) are remarkably similar to the silicate fabric estimates. For sample PP074, all three AMS eigenvectors lie within $\sim$3° of those determined for the area-weighted clinopyroxene and plagioclase fabrics. The agreement is somewhat poorer for sample PP046, although all AMS eigenvectors are broadly compatible with the silicate results. The degree of anisotropy inferred from the AMS results, however, is a poor proxy for the degree of silicate alignment. The ratios of maximum to minimum susceptibility eigenvalues ($P = 1{\cdot}05$ and 1·07, for samples PP046 and PP074, respectively) differ substantially from the values derived from direct analysis of the silicate fabric (Table 1).

The AARM tensor typically is coaxial with the silicate fabric and the magnitude of this anisotropy is often more closely related to that of the petrofabric (Fig. 19). AARM differs from AMS data in two important aspects. First, paramagnetic (and diamagnetic) phases do not contribute to AARM. Secondly, AARM faithfully records the statistical orientation of the long axes of the ferromagnetic grains, even for the finest grains that may have a more complex AMS signal (Potter & Stephenson, 1988). Remanence anisotropy results for sample PP046 (Fig. 19b) exhibit significant scatter, but the eigenvectors all are statistically indistinguishable from the AMS fabric and similar to the silicate fabrics. Specimens from sample PP074 have remarkably consistent AARM fabrics (Fig. 19d), and the mean remanence anisotropy eigenvectors agree well with both the AMS and silicate fabrics. Moreover, the degree of remanence anisotropy ($P = 1{\cdot}17$ and 2·33, for PP046 and PP074, respectively) provides a much closer match to that of the LPO fabrics from grain tracing (Table 1) and EBSD (Table 2) than does the AMS fabric. Together with the susceptibility anisotropy data, the remanence anisotropy results provide additional support for the crystallographic significance of the silicate fabrics derived from our grain-tracing technique.

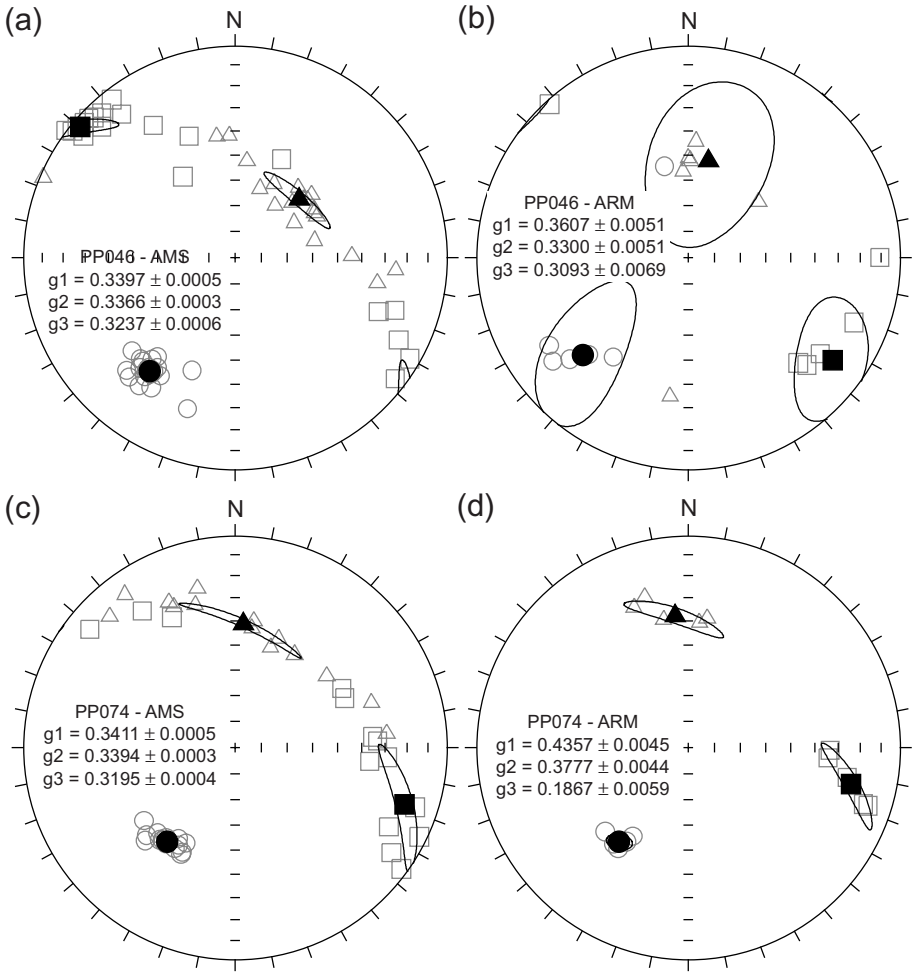

Fig. 19. Lower-hemisphere equal area plots of magnetic fabrics for samples PP046 and PP074. (a and c) AMS fabrics for individual $\sim 12\,cm^3$ minicores (grey, open symbols) and block mean (filled symbols with 95% confidence ellipses). Square, maximum; triangle, intermediate; circle, minimum. (b and d) AARM. Symbols same as for AMS plots. Eigenvalues and 1σ uncertainties shown for reference.

CONCLUSIONS

We have developed a new method for quantifying 3D silicate fabrics and, as importantly, the associated uncertainties from grain orientation data on three orthogonal sections. The orientation data for each section are represented by their CDF—the monotonic function representing the cumulative probability of a particular orientation with respect to the reference axis of the thin section. An iterative procedure is used to find the symmetric second-rank strain tensor that, when applied to a large number of unit vectors uniformly distributed on a sphere, will produce the CDFs observed on each orthogonal section. The 3D orientation matrix representing this deformed distribution provides the desired description of the fabric. Finally, a non-parametric bootstrap resampling scheme is used to provide error estimates on the eigenvectors and eigenvalues of the orientation matrix.

The CDF method has several advantages over the sectional ellipse technique often used to estimate 3D fabrics. Because the CDFs of all three sections are treated simultaneously, no arbitrary compatibility adjustments of sectional ellipses are required. The CDF technique yields a close match to the original sectional data, even for samples with well-developed fabrics that are problematic for the sectional ellipse technique. Although currently implemented for orthogonal sections, our technique is suitable for sections at any arbitrary orientation to the principal planes, requiring only knowledge of the projections onto each observation plane. The CDF method is also well suited for estimating errors and provides a direct measure of the misfit with the original orientation data. The pattern of residuals could, in principle, be used to accommodate fabrics that are not well represented by a second-rank symmetric tensor.

We have applied the technique to both traces of crystallographic features (to yield crystallographic fabrics related to the LPO) as well as grain elongation directions (to yield SPO fabrics). For pyroxenes, our grain tracings should provide an estimate of the fabric for the crystallographic *c*-axis. Although the crystallographic significance of the maximum eigenvector from tracings of the *a*–*c* plane in plagioclase is less obvious, comparison with the pyroxene fabrics from the same sample suggests that the plagioclase maximum approximates the orientation of the crystallographic *c*-axis. Direct determination of crystallographic preferred orientations from EBSD provides additional support for the crystallographic significance of the fabrics derived from grain tracings. The EBSD data corroborate the pole to foliation and the degree of anisotropy inferred from analysis of the grain tracings. Moreover, independent estimates of the volume fabric from magnetic techniques yield fabric orientations that are essentially identical to our tracing results. Analysis of grain boundary data using the CDF technique reveals a close similarity of the grain-tracing LPO and SPO fabrics, though the shape fabric may influence the magnitude of anisotropy for the grain-tracing LPO. More direct determination of the LPO from EBSD data suggests some degree of decoupling between the SPO and LPO, possibly as a result of continued crystal growth within the foliation plane (with a low degree of melt remaining) that accentuates the shape fabric, particularly the lineation within the plane of the foliation, relative to the LPO.

The CDF fabric analysis program described here is available upon request from the authors. Two versions of the program are available—one for OS9 and one for OS10 on the Macintosh. A companion program for displaying the results and error ellipses is also available.

ACKNOWLEDGEMENTS

We thank E. Meurer, C. Constable, L. Tauxe and R. L. Parker for their constructive comments during the prolonged development of the CDF technique. In particular, we are grateful to C. Constable for her suggestion to use cumulative distribution functions rather than histograms in the minimization procedure. We thank Greg Hirth, Sonja Boorman and an anonymous reviewer for helpful comments that improved the manuscript. This work was supported by NSF grants EAR9902895 and EAR9902761.

SUPPLEMENTARY DATA

Supplementary data for this paper are available on *Journal of Petrology* online.

REFERENCES

Constable, C. & Tauxe, L. (1990). The bootstrap for magnetic susceptibility tensors. *Journal of Geophysical Research* **95**, 8383–8396.

De Paor, D. G. (1990). Determination of the strain ellipsoid from sectional data. *Journal of Structural Geology* **12**, 131–137.

Efron, B. (1982). *The Jackknife, the Bootstrap, and Other Resampling Plans*. Philadelphia, PA: Society of Industrial and Applied Mathematics.

Fernandez, A. (1987). Preferred orientation developed by rigid markers in two-dimensional simple shear strain: a theoretical and experimental study. *Tectonophysics* **136**, 151–158.

Foose, M. P. (1985). Primary structural and stragraphic relations in Banded-Series cumulates exposed in the East Boulder Plateau–Contact Mountain area. In: Czamanske, G. K. & Zientek, M. L. (eds) *The Stillwater Complex: Geology and Guide. Montana Bureau of Mines and Geology, Special Publication* **92**, 305–324.

Hargraves, R. B., Johnson, D. & Chan, C. Y. (1991). Distribution anisotropy: the cause of AMS in igneous rocks. *Geophysical Research Letters* **18**, 2193–2196.

Harvey, P. K. & Laxton, R. R. (1980). The estimation of finite strain from the orientation distribution of passively deformed linear markers: eigenvalue relationships. *Tectonophysics* **70**, 285–307.

Hext, G. (1963). The estimation of second-order tensors, with related tests and designs. *Biometrika* **50**, 353–357.

Higgins, M. D. (1991). The origin of laminated and massive anorthosite, Sept Iles layered intrusion, Quebec, Canada. *Contributions to Mineralogy and Petrology* **106**, 340–354.

Higgins, M. D. (1998). Origin of anorthosite by textural coarsening: quantitative measurements of a natural sequence of textural development. *Journal of Petrology* **39**, 1307–1323.

Higgins, M. D. (2002). Closure in crystal size distributions (CSD), verification of CSD calculations, and the significance of CSD fans. *American Mineralogist* **87**, 171–175.

Hunter, R. H. (1987). Textural equilibrium in layered igneous rocks. In: Parsons, I. (ed.) *Origins of Igneous Layering*, NATO ASI Series C, Vol. 196. Dordrecht: Reidel, pp. 473–501.

Hunter, R. H. (1996). Texture development in cumulate rocks. In: Cawthorn, R. G. (ed.) *Layered Intrusions: Developments in Petrology 15*. Amsterdam: Elsevier, pp. 77–102.

Ildefonse, B., Launeau, P., Bouchez, J.-L. & Fernandez, A. (1992). Effect of mechanical interactions on the development of shape preferred orientations: a two dimensional experimental approach. *Journal of Structural Geology* **14**, 73–84.

Jerram, D. A. & Cheadle, M. J. (2000). On the cluster analysis of grains and crystals in rocks. *American Mineralogist* **85**, 47–67.

Jerram, D. A., Cheadle, M. J., Hunter, R.-H. & Elliott, M. T. (1996). The spatial distribution of grains and crystals in rocks. *Contributions to Mineralogy and Petrology* **125**, 60–74.

Lagroix, F. & Borradaile, G. J. (2000). Magnetic fabric interpretation complicated by inclusions in mafic silicates. *Tectonophysics* **325**, 207–225.

Launeau, P. & Cruden, A. R. (1998). Magmatic fabric acquisition mechanisms in a syenite: results of a combined anisotropy of magnetic susceptibility and image analysis study. *Journal of Geophysical Research* **103**, 5067–5089.

Launeau, P. & Robin, P.-Y. F. (1996). Fabric analysis using the intercept method. *Tectonophysics* **267**, 91–119.

Launeau, P., Bouchez, J. L. & Benn, K. (1990). Shape preferred orientation of object populations: automatic analysis of digitized images. *Tectonophysics* **180**, 201–211.

McBirney, A. R. & Nicolas, A. (1997). The Skaergaard layered series. Part II. Magmatic flow and dynamic layering. *Journal of Petrology* **38**, 569–580.

McCabe, C., Jackson, M. & Ellwood, B. B. (1985). Magnetic anisotropy in the Trenton Limestone: results of a new technique, anisotropy of anhysteretic susceptibility. *Geophysical Research Letters* **12**, 333–336.

McCallum, I. S., Raedeke, L. D. & Mathez, E. A. (1980). Investigations of the Stillwater complex: Part I. Stratigraphy and structure of the Banded zone. In: Irving, A. J. & Dungan, M. A. (eds) *The Jackson Volume*, *American Journal of Science* **280-A**, 59–87.

Meurer, W. P. & Boudreau, A. E. (1996). Petrology and mineral compositional features of the olivine-bearing zones of the Middle Banded series, Stillwater complex, Montana. *Journal of Petrology* **37**, 583–607.

Meurer, W. P. & Boudreau, A. E. (1998*a*). Compaction of igneous cumulates. Part I: Geochemical consequences for cumulates and liquid fractionation trends. *Journal of Geology* **106**, 281–292.

Meurer, W. P. & Boudreau, A. E. (1998*b*). Compaction of igneous cumulates. Part II: Compaction and the development of igneous foliations. *Journal of Geology* **106**, 293–304.

Nye, J. (1957). *Physical Properties of Crystals*. Oxford: Clarendon.

Potter, D. K. & Stephenson, A. (1988). Single-domain particles in rocks and magnetic fabric analysis. *Geophysical Research Letters* **15**, 1097–1100.

Press, W. H., Flannery, B. P., Teukolsky, S. A. & Vetterling, W. T. (1989). *Numerical Recipes, the Art of Scientific Computing*. New York: Cambridge University Press.

Prior, D. J., Boyle, A. P., Brenker, F., Cheadle, M. J., Day, A., Lopez, G. *et al.* (1999). The application of electron backscatter diffraction and orientation contrast imaging in the SEM to textural problems in rocks. *American Mineralogist* **84**, 1741–1759.

Ramsay, J. G. (1967). *Folding and Fracturing of Rocks*. New York: McGraw–Hill.

Rice, J. A. (1995). *Mathematical Statistics and Data Analysis*. Belmont, CA: Duxbury Press.

Robin, P.-Y. F. (2002). Determination of fabric and strain ellipsoids from measured sectional ellipses: theory. *Journal of Structural Geology* **24**, 531–544.

Scheidegger, A. E. (1965). On the statistics of the orientation of bedding planes, grain axes, and similar sedimentological data. *U.S. Geological Survey Professional Paper* **525-C**, C164–C167.

Selkin, P.A. (2003). Archean Paleointensity from Layered Intrusions. Ph.D. thesis, University of California, San Diego, 310 pp.

Selkin, P. A., Gee, J. S., Tauxe, L., Meurer, W. P. & Newell, A. J. (2000). The effect of remanence anisotropy on paleointensity estimates: a case study from the Archean Stillwater Complex. *Earth and Planetary Science Letters* **183**, 403–416.

Shimamoto, T. & Ikeda, Y. (1976). A simple algebraic method for strain estimation from deformed ellipsoidal objects: 1. basic theory. *Tectonophysics* **36**, 315–337.

Stephenson, A. (1994). Distribution anisotropy: two simple models for magnetic lineation and foliation. *Physics of the Earth and Planetary Interiors* **82**, 49–53.

Uyeda, S., Fuller, M. D., Belshe, J. C. & Girdler, R. W. (1963). Anisotropy of magnetic susceptibility of rocks and minerals. *Journal of Geophysical Research* **68**, 279–291.

Waters, C. & Boudreau, A. E. (1996). A reevaluation of crystal-size distributions in chromite cumulates. *American Mineralogist* **81**, 1452–1459.

Watson, G. S. (1966). The statistics of orientation data. *Journal of Geology* **74**, 786–797.

Wheeler, J. (1986). Average properties of ellipsoidal fabrics: implications for two- and three-dimensional methods of strain analysis. *Tectonophysics* **126**, 259–270.

Woodcock, N. H. (1977). Specification of fabric shapes using an eigenvalue method. *Geological Society of America Bulletin* **88**, 1231–1236.

Xu, W., Geissman, J. W., Van der Voo, R. & Peacor, D. R. (1997). Electron microscopy of iron oxides and implications for the origin of magnetizations and rock magnetic properties of Banded Series rocks of the Stillwater Complex, Montana. *Journal of Geophysical Research* **102**, 12139–12157.

Zieg, M. J. & Marsh, B. D. (2002). Crystal size distributions and scaling laws in the quantification of igneous textures. *Journal of Petrology* **43**, 85–101.

APPENDIX

Although the method of fabric analysis using cumulative distribution functions (CDFs) is conceptually simple, a number of steps are involved in generating the 3D fabric and error estimates. The basic steps in the CDF method are illustrated in the flow chart (available as online supplementary material) and additional details of the implementation of this method are briefly described below.

The Nelder–Mead simplex multivariate minimization technique (Press *et al.*, 1989) is used to iteratively solve for the six independent elements of the symmetric second-rank strain tensor that will minimize the misfit with all three CDFs. The starting tensor for the minimization is an isotropic one (i.e. diagonal elements are 1/3 and off-diagonal elements are 0). The best-fit strain tensor is then used as the starting point for a second minimization. This refinement typically results in only a modest change in the best-fit tensor (a few parts in 10^4 for each tensor element), suggesting that the final result is near a global minimum. Although the CDFs for each section require no binning of data, practical considerations demand that the CDFs be evaluated at a consistent number of points. No detectable differences in the final tensor were found for evaluation at intervals of 0·5° and 1·0°. The latter value was therefore used for all results in this paper.

The validity of the orientation matrix obtained from the simplex minimization depends, to some extent, on the uniformity of the starting distribution of unit vectors. Although approximately uniform distributions on a sphere can be produced by a variety of methods, we have found that distributing points on a series of regularly spaced rings with constant z value (i.e. latitudinal rings) provides suitably uniform distributions (Fig. 1a). The spacing of points on each ring is chosen to most closely match the spacing of the rings. The orientation matrix for the resulting distribution of vectors provides a measure of the uniformity of the distribution. With 60 or more rings, the orientation matrix closely approximates that of a uniform distribution (diagonal terms = 1/3 and all off-diagonal terms = 0). For all the results in this paper, a uniform distribution with 66 rings and 5550 points has been used. The orientation matrix of this distribution differs from the ideal uniform case by, at most, 1 part in 10^5.

Error estimates for both the eigenvalues and eigenvectors of the orientation matrix are based on 500

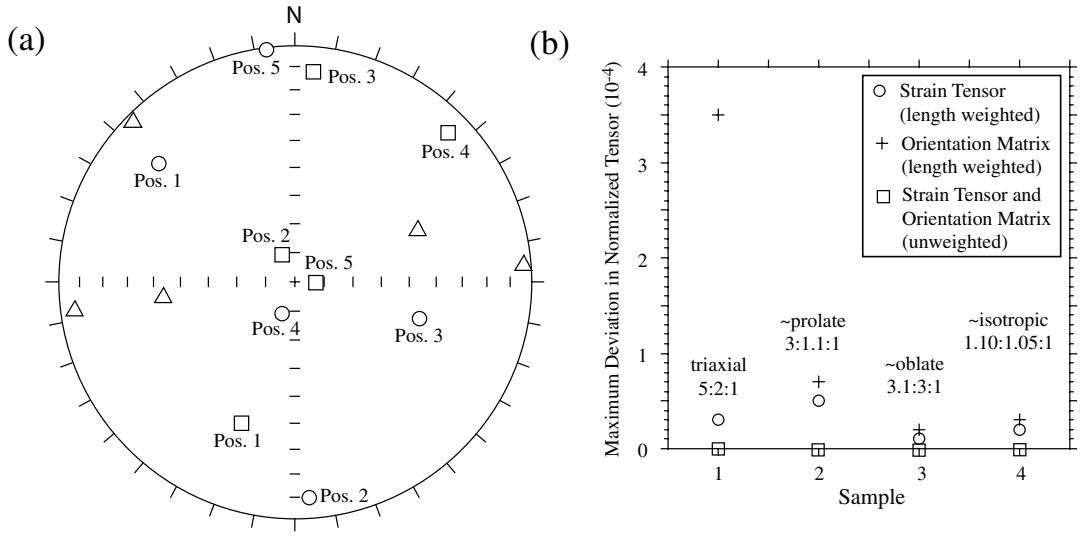

Fig. A1. Synthetic results illustrating that CDF method (unweighted or length-weighted analysis) accurately recovers both the strain tensor and orientation matrix. (a) Equal area plot showing the eigenvectors of test strain tensors in each of the five test orientations. □, eigenvector associated with maximum eigenvalue; △, intermediate; ○, minimum. Test thin sections are parallel to the coordinate axes. (b) Maximum deviation of the recovered strain tensor or orientation matrix relative to the known value.

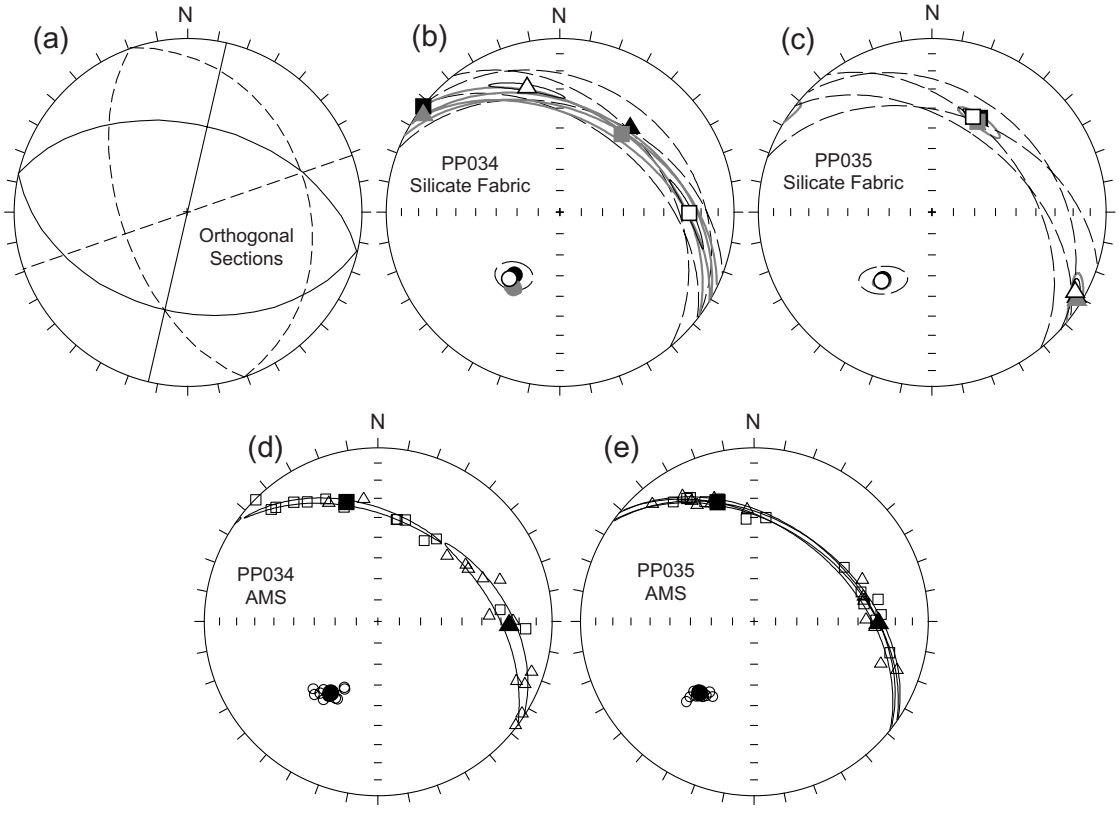

Fig. A2. Silicate fabric and AMS results from two adjacent block samples with distinct field orientations. (a) Equal area plot showing the lower-hemisphere traces of the orthogonal thin sections for sample PP034 (continuous lines) and sample PP035 (dashed lines). (b) Length-weighted fabric for all mineral phases for sample PP034. Plagioclase results shown by open symbols and continuous lines; clinopyroxene (grey); orthopyroxene (black with dashed 95% confidence bounds). (c) Fabric results for sample PP035 [same conventions as for (b)]. (d) AMS data for sample PP034. Individual minicore results shown by smaller, open symbols. Filled symbols and ellipses indicate the sample mean directions and 95% error bounds. (e) AMS data for sample PP035 [same conventions as for (d)]. Square, maximum; triangle, intermediate; circle, minimum. All plots are in geographic coordinates.

pseudosamples drawn from the original data. A smaller number of pseudosamples could potentially be used in some cases (e.g. samples with well-developed fabrics and with a large number of observations available on each section). Deviations between the eigenparameters of the best-fit orientation matrix and those of the mean orientation matrix determined from all pseudosamples are an indication that a larger number of pseudosamples should be used. Eigenparameters in the figures in the text are from the mean of the pseudosamples. Comparison with the results in Table 1 (from the best-fit orientation matrix) reveals minor differences in some cases, indicating that 500 pseudosamples are sufficient in most cases.

The CDF technique described in the text is suitable for description of the preferred orientation of linear features (either treated as unit vectors or weighted by vector length) and is ideal for strain analysis based on passive linear markers. In addition, the iterative forward modeling approach should be suitable for arbitrarily oriented sections relative to the fabric ellipsoid. In order to test the validity of the method on arbitrarily oriented thin sections and the use of lengths in weighting the data, we generated synthetic 2D orientation data on three orthogonal sections from a deformed 3D distribution of vectors produced by applying a known strain tensor to a uniform distribution of unit vectors (and, hence, with a known orientation matrix for the deformed distribution). Four test strain tensors (approximately isotropic, oblate, prolate and tri-axial) and five orientations of the strain tensor relative to the thin sections were used (Fig. A1a). When the 2D orientation data are treated as unit vectors, both the strain tensor and orientation matrix are recovered exactly (Fig. A1b). For the case of length-weighted orientation observations, the recovered strain tensor and orientation matrix typically differ from the true values by less than 1 part in 10^4.

As an additional test of the validity of the CDF method for arbitrarily oriented thin sections, we have determined silicate fabrics for two adjacent block samples. These two blocks (gabbronorites from the Middle Banded Series, Picket Pin Mt) were collected from approximately the same stratigraphic level (within $\sim$10 cm) and were separated laterally by about 25 cm. The orientations of the field-drilled cores used to orient each block were significantly different, as illustrated by the traces of the resulting orthogonal thin sections (Fig. A2a).

Despite the very different orientations of the thin sections, the poles to the foliation determined from all mineral phases from both samples agree within a few degrees (Fig. A2b and c). The degree of anisotropy is also quite similar. For sample PP034, the plagioclase fabric ellipsoid (eigenvalues of 0·488, 0·422, 0·090; all results are for length-weighted analysis) indicates a strong foliation, though with a statistically significant lineation. The eigenvalues for the clinopyroxene (0·457, 0·434, 0·109) and orthopyroxene (0·446, 0·427, 0·127) are slightly less anisotropic and statistically oblate, as indicated by the 90° half angles of the 95% confidence ellipses. Sample PP035 yields a slightly more tri-axial plagioclase fabric (0·521, 0·384, 0·095). The clinopyroxene fabric is also tri-axial (0·494, 0·390, 0·116), with eigenvectors that agree well with those determined from the plagioclase grains for this sample. The orthopyroxene fabric for sample PP035 (0·452, 0·396, 0·152) is statistically oblate.

Though these two samples yield very similar results for the pole to foliation and degree of anisotropy, the eigenvectors associated with the maximum and intermediate eigenvalues for plagioclase differ significantly. This discrepancy may indicate real variability in the fabric lineation. Both samples were taken in a portion of the Middle Banded Series characterized by the presence of plagioclase 'clots' (polycrystalline aggregates of blocky plagioclase up to several cm in size) that may significantly affect the local fabric (Foose, 1985; Meurer & Boudreau, 1998*b*). AMS results from these two block samples (Fig. A2d and e) also suggest that only a weak, and quite variable, lineation is present. Overall, the results support the validity of the CDF technique applied to arbitrarily oriented sections, though the presence of plagioclase clots makes this test less than ideal. Alternatively, the discrepancy between the plagioclase lineation directions of the two blocks may reflect limitations in defining the clustering of plagioclase *c*-axes from tracings of the *a*–*c* plane.